AD-A129 166 OPTICAL COMPUTING RESEARCH(U) STANFORD UNIV CA STANFORD 1/1
ELECTRONICS LABS J GOODMAN ET AL. 31 MAR 83
AFOSR-TR-83-0494 AFOSR-82-0089

UNCLASSIFIED F/G 20/6 NL

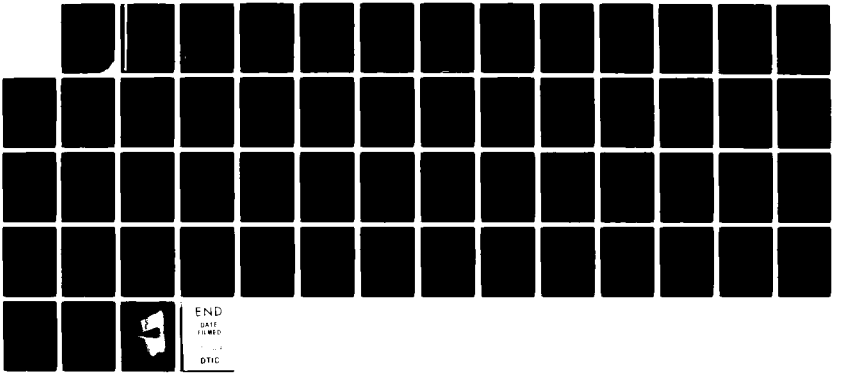

END
DATE FILMED
DTIC

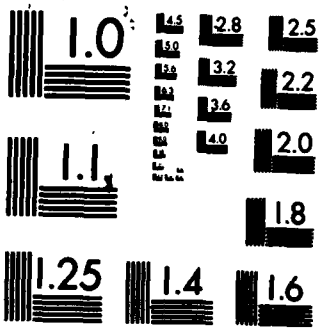

INFORMATION SYSTEMS LABORATORY

STANFORD ELECTRONICS LABORATORIES
DEPARTMENT OF ELECTRICAL ENGINEERING
STANFORD UNIVERSITY · STANFORD, CA 94305

OPTICAL COMPUTING RESEARCH

Joseph W. Goodman
Lambertus Hesselink
Qizhi Cao
Raymond Kostuk
Ellen Ochoa
Rae-Hong Park

March 1983

Annual Technical Report Number L722-8

Research supported by the Air Force Office of Scientific Research, Air Force Systems Command, USAF, under Grant No. AFOSR 82-0089. The United States Government is authorized to reproduce and distribute reprints for governmental purposes, notwithstanding any copyright notation hereon.

Information Systems Laboratory
Stanford Electronics Laboratory
Stanford University, Stanford, California

UNCLASSIFIED

SECURITY CLASSIFICATION OF THIS PAGE (When Data Entered)

REPORT DOCUMENTATION PAGE	READ INSTRUCTIONS BEFORE COMPLETING FORM
1. REPORT NUMBER AFOSR-TR- 83-0494 2. GOVT ACCESSION NO. AD-A129166	3. RECIPIENT'S CATALOG NUMBER
4. TITLE (and Subtitle) OPTICAL COMPUTING RESEARCH	5. TYPE OF REPORT & PERIOD COVERED Annual Report 2-1-82 - 1-31-83
	6. PERFORMING ORG. REPORT NUMBER
7. AUTHOR(s) Joseph Goodman, Lambertus Hesselink, Qizhi Cao, Raymond Kostuk, Ellen Ochoa, Rae-Hong Park	8. CONTRACT OR GRANT NUMBER(s) AFOSR.82-0089
9. PERFORMING ORGANIZATION NAME AND ADDRESS Stanford University Stanford, CA 94305	10. PROGRAM ELEMENT, PROJECT, TASK AREA & WORK UNIT NUMBERS 61102F 2305/B1
11. CONTROLLING OFFICE NAME AND ADDRESS United States Air Force Air Force Office of Scientific Research Bldg. 410, Bolling AFB, DC 20332	12. REPORT DATE March 31, 1983
	13. NUMBER OF PAGES 54
14. MONITORING AGENCY NAME & ADDRESS(if different from Controlling Office) As above	15. SECURITY CLASS. (of this report) Unclassified
	15a. DECLASSIFICATION/DOWNGRADING SCHEDULE

16. DISTRIBUTION STATEMENT (of this Report)

Approved for public release; distribution unlimited.

17. DISTRIBUTION STATEMENT (of the abstract entered in Block 20, if different from Report)

18. SUPPLEMENTARY NOTES

19. KEY WORDS (Continue on reverse side if necessary and identify by block number)

optical computing
optical data processing

20. ABSTRACT (Continue on reverse side if necessary and identify by block number)

This document contains information on the research accomplished under AFOSR Grant No. AFOSR 82-0089 during the time period February 1, 1982 through January 31, 1983. The work covers several different areas of optical computing, as well as some work on digital processing of optically obtained images.

DD FORM 1 JAN 73 1473

UNCLASSIFIED

SECURITY CLASSIFICATION OF THIS PAGE (When Data Entered)

OPTICAL COMPUTING RESEARCH

Joseph W. Goodman
Lambertus Hesselink
Qizhi Cao
Raymond Kostuk
Ellen Ochoa
Rae-Hong Park

March 1983

Annual Technical Report
Report Number L722-8

Research supported by the Air Force Office of Scientific Research, Air Force Systems Command, USAF, under Grant No. AFOSR 82-0089. The United States Government is authorized to reproduce and distribute reprints for governmental purposes, not withstanding and copyright notation hereon.

Information Systems Laboratory
Stanford Electronics Laboratory
Stanford University, Stanford, California

ABSTRACT

This document contains information on the research accomplished under AFOSR Grant No. AFOSR 82-0089 during the time period 1 February 1982 through 31 January 1983. The work covers several different areas of optical computing, as well as some work on digital processing of optically obtained images. The primary emphasis of the work is on the possible applications of optics to interconnections in integrated circuit technology. Other areas of effort include the diagonalization and inversion of circulant matrices using coherent optics, the division of complex wavefronts using four-wave mixing, and the suppression of speckle in coherently formed images. Publications during the last year arising out of work supported by the grant are also detailed.

I. INTRODUCTION

This report covers the work performed on AFOSR grant No. 82-0089 during the time period 1 February 1981 through 31 January 1982. It is divided into six sections, the first of which is this Introduction. Immediately following we summarize our current status of the project aimed at investigating the applications of optics to the interconnection problem in integrated circuit technology. Section III deals with the results of our work on the use of coherent optical processing for the diagonalization and inversion of circulant matrices. Section IV discusses a new project started this year, namely one concerned with the possibility of performing complex wavefront division using four-wave mixing. Section V reports the early results of another new project, one aimed at suppressing speckle in coherently formed images by means of digital image processing techniques. Finally, section VI details the publications and meeting presentations arising out of work supported by the grant during the past grant year.

II. OPTICAL INTERCONNECTIONS FOR VLSI

As integrated circuit technology advances, device sizes are being reduced at the same time that overall chip sizes increase. The increased complexity of such chips places ever increasing demands on interconnect technology. The RC time delays and IR voltage drops of conventional aluminum and polycrystalline silicon interconnections may ultimately eclipse the gains anticipated in device performance.

This project is concerned with the possibility of using optical imaging interconnections to overcome some of the problems imposed by current interconnect technology. The substitution of optical waveguides for metallic interconnection lines could potentially reduce the effects of RC time delays and IR voltage drops now experienced. However, our goal is to evaluate the feasibility of using optical interconnects that rise above the chip, rather than simply using waveguides to mimick the quasi-planar topology of conventional interconnections. We envision the use of holographic optical elements, either transmissive or reflective, to provide a multitude of non-interfering, efficient parallel communication channels, either into a chip from the outside world or between two chips. Eventually the problem of providing interconnects within a single chip would also be of interest. Since the particular interconnect pattern achieved is determined by the holographic optical element used, there exists the tantalizing possibility of dynamically changing the interconnect pattern to meet the current needs of the processor performing the computations on the chip.

Of the various problems that could be tackled, that of communicating by means of optics from the outside world into a chip appears to be the most amenable to current technological solution. For such problems, there need be no flow of optical information out of the chip, and hence the difficult problem of providing on-chip optical sources or modulators is avoided. Considerable time was wasted in the early part of this project in attempting to find ways to integrate small liquid crystal light modulators on a silicon chip. It was finally concluded that, while the goal was probably achievable with considerable work, the speed

of the resulting modulators would be so slow that there would be little interest in the end result.

Providing detectors on the chip poses no fundamental problem. As the complexity of chips grows, the needs for connections into the chip also grows. Yet current pin-connecting approaches are generally limited to providing on the order of 100 connections to the outside world. The success of optics in meeting these needs will depend critically on the size and performance of the detectors that can be realized on the chip, and on the stringent positioning tolerances between the imaging element and the chip.

Our work on the imaging interconnect problem has three separate aspects. One deals with the optical issues associated with the interconnect devices (holograms), and the second with the on-chip photodetectors that provide the means for inputting data. The third consists of a continuing search for algorithms and specific problems that demand input of large amounts of data in parallel (while requiring rather smaller output capability). A fourth aspect, that of finding ways to place optical sources on chips, is viewed as a longer-range goal and is under study in the Integrated Circuits Laboratory under separate support. It should be mentioned that some experts in this field feel that in the long term a solution to this difficult device problem will be found, possibly by using a buffer material (such as germanium) between silicon and gallium arsenide to provide adequate matching of the lattice dimensions.

It is attractive, for reasons of cost and simplicity, to consider light-emitting diodes (LED's) as prime candidates for the modulated sources that will be used for the optical communication channels into the chip. However, the spectral purity of LED's is far poorer than that of lasing diodes, and therefore some understanding of the resolution of holographic optical elements when used with LED sources must be gained. As a goal towards this end, a system has been under construction which we hope will provide a test bed for answering questions of this kind. Also to be gained from these experiments is knowledge about the

scattering of light by the holographic optical elements and by the silicon chip itself. A number of GaAsP unbonded LED's were obtained from Hewlett Packard, and mounted in an array format on a DIP package. Several encapsulating materials are being examined to determine which will minimize light scattering and beam distortion and provide environmental protection. Hewlett Packard also supplied a number of unbonded silicon photodetectors of the type used in electro-optic couplers. These have also been mounted in DIP packages and will be calibrated and used to test S/N and response threshold levels. A Fairchild I-scan CCD line scanner will be used to monitor images in the hologram image plane. Initially, transmission and reflection type holograms will be prepared using conventional sources, geometries and films. Later, experiments will be conducted with image plane holographic geometries and dichromated gelatin recording materials. These systems have promising white-light reconstruction and high diffraction efficiency characteristics.

Preparations for these experiments have now been largely completed and the experiments themselves are anticipated to be under way in the very near future. In the meantime the problem of integrating photodetectors onto the chip will be under study in parallel. Initial efforts in this regard will be aimed at studying fundamental limits to the size, speed and sensitivity of these devices. Our approach is to identify the problems that are anticipated when attempting communication into a chip, and to gather the information necessary to assess the seriousness of these problems in a methodical way. We intend to focus attention on fundamental issues, such as the radiometry of the problem, which determines the available light power at the detectors, and the fundamental limits to detector size and sensitivity.

Finally we mention a new concept that has arisen during the past grant year. Consider a single source of information that must be supplied to a number of sites on a chip. Further suppose that the algorithm being realized on the chip requires that bursts of information be sent to different sites on the chip (i.e. with different interconnect patterns) as a function of time. Such requirements can be met in the following way. A single high-speed optical channel is to be fed into

the chip, but it should be interconnected to different sets of locations on the chip as a function of time. We can satisfy such a requirement by use of an acousto-optic beam deflector, and a two-dimensional array of holographic optical elements, each providing a different interconnect pattern. The hologram functions much as a holographic memory. To address a particular set of desired points on the chip, the acousto-optic deflector sends the beam to the particular location on the hologram; the image read out is a series of spots at the desired locations on the chip, where detectors convert the burst of high-speed optical modulation into electrical signals. The beam deflector then sends the light to another hologram in the array, which then sends a new set of light spots to presumably another set of detectors on the chip, where the new burst of information is converted to electrical signals.

The concept described above appears to be a powerful one, but the missing link at present is the lack of any well-defined problem or algorithm that requires this type of communication. Nonetheless, we feel confident that such algorithms can be found, and we will be searching for examples during the coming grant year.

III. COHERENT OPTICAL TECHNIQUES FOR DIAGONALIZATION AND INVERSION OF CIRCULANT MATRICES.

For the past year we have been studying the possible use of coherent optical systems for diagonalization and inversion of circulant matrices. Circulant matrices are those for which each successive row is a simple circular shift of the row above by a single element. For example, in the matrix A below, the numbers 1,2,3, and 4 stand for four distinct elements; the organization of those elements in the circulant matrix is as follows:

$$A = \begin{matrix} 1 & 2 & 3 & 4 \\ 4 & 1 & 2 & 3 \\ 3 & 4 & 1 & 2 \\ 2 & 3 & 4 & 1 \end{matrix} \qquad (1)$$

A remarkable property of circulant matrices is that they are diagonalized by the discrete Fourier transform (DFT), the resulting diagonal elements being the complex eigenvalues of the original matrix. Thus if the DFT matrix W is defined by (again illustrating with a 4x4 example)

$$W = \begin{matrix} 1 & 1 & 1 & 1 \\ 1 & w & w^2 & w^3 \\ 1 & w^2 & w^4 & w^6 \\ 1 & w^3 & w^6 & w^9 \end{matrix} \qquad (2)$$

where $w = \exp(-i2\pi/N)$, we have

$$\Lambda = W^{-1} A W = \begin{matrix} \lambda_1 & 0 & 0 & 0 \\ 0 & \lambda_2 & 0 & 0 \\ 0 & 0 & \lambda_3 & 0 \\ 0 & 0 & 0 & \lambda_4 \end{matrix} \qquad (3)$$

where the λ's are the eigenvalues of A.

Before embarking on a more detailed description of the work, it is perhaps worthwhile addressing the question why would anyone want to

diagonalize circulant matrices, and why might coherent optics be a useful approach in some cases. A great many signal processing problems require the inversion of Toplitz correlation matrices. Toplitz matrices have less structure than circulant matrices; they simply have the property that each subdiagonal of the matrix has elements that are identical. Such matrices must be inverted in order to determine the structure of optimal linear filters, and such inversions must be performed frequently in environments where the statistics are changing with time or are gradually becoming known as time progresses. Usually the Toplitz matrices of concern are banded matrices; that is only the main diagonal and a few subdiagonals have significant non-zero value. It can be shown that a large banded Toplitz matrix can be inverted by first inverting a large circulant approximation to that matrix, followed by inversion of a much smaller Toplitz matrix [Ref. 1]. Hence the availability of a fast optical technique for inverting large circulant matrices, together with a digital processor that inverts a small Toplitz matrix, allows large Toplitz matrices to be inverted, hopefully with greater speed than afforded by an all-digital approach. Once a method for diagonalizing circulant matrices optically is in hand, then methods exist for inverting such matrices, as we describe later.

There is an additional reason for interest in the problem of inverting circulant matrices optically. In working with matrices, rather than pictorial data, one is dealing with numbers, and the results of the processing operation are likewise numbers. It therefore becomes rather easy to assess the accuracy of the operations one is performing, and to discover the primary sources of accuracy limitation in the system. Thus we regard this project as providing a testbed within which the sources of inaccuracy of coherent optical processors can be studied in a more precise way than has been possible before. Knowing the chief reasons for inaccuracies allows one to focus attention on these sources of error and to explore methods for reducing their effects. Thus information discovered in this project may have wider application in the field of coherent optical processing.

With this information as background, we return to a more detailed

discussion of the optical problem. The task of diagonalizing a circulant matrix using coherent optics can be performed if the normal continuous two-dimensional Fourier transform so easily performed by such systems can be changed to a discrete Fourier transform. Much of our work on this project during the past year has been aimed at conversion to a discrete Fourier transform. The method used for this conversion is as follows. The matrix to be diagonalized is entered into the coherent optical system as an array of transmitting cells in a mask. The matrix is repeated at least 3 by 3 times in the horizontal and vertical directions, causing the spectrum to form a series of discrete spots. Each of these spots represents a different complex eigenvalue of the original matrix. Measurement of the intensities of these spots by discrete elements of a detector array is equivalent to measurement of the squared magnitudes of the eigenvalues of the matrix. If the full complex values are desired, then interferometry or heterodyne detection must be used to extract both amplitude and phase information.

A major component of our effort during the past year has been aimed at an analysis of this method for performing the discrete Fourier transform. The analysis examined the effects of the repetitions of the matrix at the input plane, the finite cell sizes used to represent matrix elements, and the finite sizes of the detector elements used to measure the eigenvalues. It was discovered that the operation performed by the two-dimensional system is not quite that indicated in Eq. (3) above. The inverse operation associated with the first W matrix is missing in the optical realization, and as a consequence the locations of the spots representing the eigenvalues of interest are not quite those expected at the start. Nonetheless, the desired spots are present and must simply be detected in the correct region of the output.

Figure 1 below shows the optical setup used for obtaining eigenvalues, a sketch of a typical matrix transparency introduced into the system (for a 4x4 case), and a sketch of the resulting distribution of light intensity in the focal plane of the lens. Note that there is are a large number of light spots in the output. Those representing the eigenvalues of interest are enclosed in a box.

During the past year we have discovered a simple technique for entering circulant matrices with complex elements into the system. Matrices representing the biased real part and the biased imaginary part are interlaced with a diagonal spatial offset of one quarter of a cell separation distance. The biases do not affect the output provided the eigenvalues are detected in a subdiagonal that does not contain the zero-frequency or "D.C." spot. The spatial offset of the real and imaginary part matrices results in the complex addition of their respective eigenvalues with a 90 degree phase shift. As a consequence the eigenvalues of the complex matrix are detected. The technique is illustrated in Figure 2.

The chief accuracy limitations we have encountered so far in measuring eigenvalues by these methods have arisen from inaccuracies of the optical masks representing the input matrices. These masks have been written on a DICOMED plotter at the NASA Ames Research Center. It was necessary for us first to calibrate the gray levels of the plotter. Following this, we discovered that the spot sizes written by the plotter are a function of the gray level being written, and further calibration had to be done. Finally we turned to having the masks fabricated in our Integrated Circuits Laboratory. Preliminary results with one such mask show that most of the limitations we were encountering with the transparencies written with the DICOMED plotter are no longer present. In our latest experiment, using only a 3x3 matrix, an accuracy of 1.5% was obtained in the measured eigenvalues. This accuracy may be a function of matrix size, a point to be explored in the future. We are also obtaining some transparencies written with an electron beam lithography machine, and will be evaluating them for accuracy.

At this point it appears that our major problems in producing masks that accurately represent the matrices of concern have been overcome, and that future efforts can be more directly aimed at inaccuracies arising within the coherent optical processing system itself.

Attention will be turning later this year away from the measurement

of eigenvalues towards the inversion of circulant matrices. In order to invert such matrices, it is necessary to record the complex eigenvalues in the focal plane holographically, and to produce a transparency with complex amplitude transmittance proportional to the reciprocal of the complex fields associated with the original eigenvalues. A second discrete Fourier transform will produce an output matrix that is the inverse of the original matrix. The necessary nonlinearities can be achieved with photographic film using the techniques that have been developed in the past for coherent optical inverse filtering. We intend to do our work with such methods, although our interest will also be focused on possible techniques for performing the same operations in real time without the use of photographic film. One such technique is the subject of study in another project supported by this grant and described in the section that follows.

A paper describing our past work on this project will be presented at the forthcoming International Optical Computing Conference.

IV. WAVEFRONT DIVISION BY FOUR-WAVE MIXING

A new project begun during the past year is aimed at using four-wave mixing to divide one complex wavefront by another complex wavefront. Past work by others has indicated that, under certain conditions, the strength of the signal generated in a degenerate four-wave mixing experiment is proportional to the contrast of the fringes between the object wave and one of the pump waves [Ref. 2]. Workers in holography have shown that under such conditions holograms can be used to perform a division between a complex wavefront incident on the hologram during reconstruction and the complex object wavefront stored in the hologram [Ref. 3]. The idea carries over directly to four-wave mixing, in which the wavefront incident in the probe beam will be divided by the wavefront carried by one of the pump beams. The chief experimental difficulty is that, with currently available materials (e.g. BSO) used in the way necessary to achieve division, the reflected wave of interest is extremely weak. This problem may be solved with the availability of

crystals with higher efficiency and even gain, but for the moment the ideas must be tested with BSO.

A major effort has been mounted during the past year to develop the instrumentation needed to measure the relevant properties of BSO at the very low light levels anticipated. This work has involved the interfacing of our Reticon array to a microcompter through A/D converters in such a way that a large number of measurements can be made, the results digitized, and the measurements averaged to increase the signal to noise ratio. At this point the interfacing is done, but the Reticon array electronics are being repaired after a failure. It should not be too long until we can take the measurements needed to ascertain the dynamic range over which wavefront division can be achieved.

In the meantime we have been developing ideas regarding possible applications of real-time wavefront division to practical problems. One fairly obvious application is to inverse filtering or image deblurring, and indeed the method could be used for inversion of circulant matrices, and discussed in the previous section. We have also developed some ideas about how to use the method in the testing of integrated circuit masks for defects, but it is a bit too early to discuss these ideas at this point.

As part of our effort to become more familiar with the mathematics of four-wave mixing, we undertook a study of what diffraction efficiencies could be achieved when the object beam contains a speckle pattern, as it would for any diffuse object. Relevant work in holography was found [Ref. 4], but it was discovered that an important effect was left out of that analysis that should have been included. This effect arises from the random tilts of the wavefront (associated with the speckle phenomenon) and the resulting random tilts of the fringes of the interference patterns in the crystal. These tilts affect the diffraction efficiency that can be achieved. It was necessary to develop further information on the statistics of wavefront tilt in a speckle pattern. Such an analysis was carried out, and based on it, a paper was submitted to the Journal of the Optical Society of America. This paper has now

been accepted and will appear in the July issue. A copy is appended to this report.

The major emphasis of our work in the immediate future will be aimed at collecting the necessary experimental data that will tell us information concerning the validity of the ideas about wavefront division. After the limitations of the method are fully understood, attention will be devoted to studies of potential applications of the method.

V. STUDIES OF SPECKLE SUPPRESSION ALGORITHMS

Another new effort initiated during the past year has been in the area of speckle suppression in coherently formed images. Speckle arises whenever an object containing surface roughness on the scale of the illuminating wavelength is imaged. Speckle occurs in synthetic aperture radar images, in medical ultrasound images, and milimeter waves images, for example. Any method that would suppress this disturbing noise without while preserving resolution for the desired object information would constitute a major contribution.

Many methods for suppressing speckle have been studied in the past. The most obvious method is simply to blur the intensity distribution in the image with some kind of linear filter, in which case not only is speckle reduced, but also the desired portion of the image is blurred with a consequent loss of resolution. The key question to be addressed is whether there exists another approach to speckle suppression that does better than simple blurring in terms of the tradeoff between speckle noise and resolution. Unfortunately, many recent studies of speckle suppression have not compared the results obtained with those achievable by simple blurring, and therefore it is not fully possible to judge the merits of these techniques.

In beginning our work in this area, it was first necessary to develop accurate methods for simulating the speckle phenomenon

digitally. The problem is far more difficult than might be imagined at first glance. Simple random phase coding of the object, followed by low-pass filtering in the frequency domain, yields as serious problem with aliasing. Our approach has been to convolve a randomly phase-coded object with an accurate representation of the amplitude spread function of the imaging system, without resorting to discrete Fourier transforms at all. Excellent results have been obtained for one dimensional objects, and we are now extending the method to two dimensions.

The speckle suppression methods studied (so far primarily in one dimension) have been the following:

1. Simple blurring of the intensity image by a rectangular spread function.

2. Filtering of the image intensity with a linear Wiener filter designed for multiplicative noise.

3. Logarithmic or homomorphic filtering, in which the logarithm of the image intensity is smoothed with a rectangular point-spread function, following which exponentiation of the image is performed.

4. Median filtering, in which the median of the image intensity values within a moving rectangular window is chosen as the value of the filtered image at each point. Several iterative passes through such filter ultimately yield a so-called "root" image [Ref. 5], which likewise has been studied as a possible restoration of the speckled image.

5. Maximum entropy processing, an approach not studied before in speckle suppression, and adapted to this problem by us. More explanation of the method is presented below.

In all cases we used the mean-squared error between the filtered image and an "ideal" image as the criterion of goodness. For the "ideal" image we considered both the intensity distribution in the

coherently formed image (obtained from a system with the same limiting pupil) and the intensity distribution of the incoherently formed image (again through the same system). The results indicated that all restoration techniques produce images that are closer to the incoherently formed image than to the speckle-free coherently formed image.

The maximum entropy approach to speckle suppression is based on the following ideas. The image intensity has a Fourier transform that is identically equal to the deterministic autocorrelation function of the fields incident on the pupil of the imaging system. Thus the problem of estimating the image intensity in the presence of speckle can be regarded as a kind of spectral estimation problem, in which we are trying to estimate the power spectral density of a random process from one sample function of that process. If we were able to exactly estimate the power spectral density of the underlying random process, we would be able to Fourier transform that result and obtain a speckle-free image with full the resolution of the imaging system.

At low spatial frequencies (small separations in the pupil autocorrelation process), a great deal of spatial averaging is performed, and the spectral density obtained from a single sample function (i.e. a single speckled image) is very close to the value that would be obtained from an average over an ensemble of images. However, at high spatial frequencies relatively little spatial averaging occurs, and the power spectrum associated with the single speckled image departs significantly from that associated with an ensemble average. The maximum entropy approach simply throws away the high spatial frequencies in the spectrum, retaining the low spatial frequencies, and attempts to estimate the high-frequency portion of the spectrum from the low frequency portion using the maximum entropy method. Details about this method will be presented in a future publication; for the present the above description should suffice.

Our results to date indicate that the best restorations (best meaning least mean-squared error) are obtained with a linear Wiener

filter based on the multiplicative model of speckle. Second in performance is the maximum entropy method. A very close third is simple linear averaging with a rectangular window. Rather far behind in performance are both homomorphic filtering and median filtering.

Criticisms that can be leveled at these results are two-fold. First, the results to date are one-dimensional, and the ordering of performance could conceivably be different in two dimensions. Second, only a limited set of objects have been studied, and the results may be object-dependent. We believe that neither of the criticisms will turn out to be valid, but further work is necessary to verify this belief.

The maximum entropy method used is a rather crude one, and we intend to test other more sophisticated versions of this approach. The project is ultimately a sufficiently large one that we intend to seek other support to carry it on. Hopefully by Autumn of this year other support will be in hand. However, AFOSR will continue to receive credit for their initial support of the work, without which it could not have begun.

VI. PAPERS PUBLISHED AND MEETING PRESENTATIONS

We summarize in this section the various publications and presentations made during the past year reporting on work supported by this grant.

A. Papers Published

J.W. Goodman and Moon Song, "Performance limitations of an analog method for solving simultaneous linear equations", APPLIED OPTICS 21, 502-506 (1982).

M. Tur, K-C Chin, and J. W. Goodman, "When is speckle noise multiplicative?", APPLIED OPTICS 21, 1157-1159 (1982).

J.W. Goodman, Architectural development of optical data processing systems" (invited), J. E. E. E. AUSTRALIA 2, 139-149 (1982).

B. Papers Accepted for Publication

E. Ochoa and J.W. Goodman, "Statistical distribution of Ray-directions in a fully developed speckle pattern" (accepted for publication in J. Opt. Soc. Am.)

C. Oral Presentations

J.W. Goodman, "Architectural development of optical data processing systems", Conference on lasers and electro-optics, Phoenix, Arizona, May, 1982 (invited).

J.W. Goodman, "Optical data processing, past, present and future", Conference on Electrooptics, Tokyo, Japan, December 1982 (invited).

Finally, the contributions of various individuals should be explicitly mentioned. Prof. L. Hesselink provided advice and encouragment for various graduate students involved with the grant. Dr. Moshe Tur provided guidance for graduate students working on various problems described above. Work on optical interconnections has been performed primarily by Raymond Kostuk. Work on diagonalization and inversion of circulant matrices was performed by Q. Cao. Work on wavefront division using four-wave mixing was performed by E. Ochoa, who was also partially supported by an IBM doctoral fellowship. Work on speckle suppression was performed by Rae-Hong Park.

REFERENCES

1. Anil K. Jain, "Fast inversion of banded Toplitz matrices by circulant decompositions, IEEE Trans. ASSP, ASSP-26, April 1978.

2. Jeffry O. White and Amnon Yariv, "Real-time image procesing via four-wave mixing in a photorefractive medium", Appl. Phys. Lett. 37, 1980.

3. S.I. Ragnarsson, Physica Scripta 2, 145 (1970).

4. Juris Upatnieks and Carl Leonard, "Efficiency and image contrast of dielectric holograms", J. Opt. Soc. Am. 60, 297 (1970).

5. Thomas A. Nodes, Neal C. Gallagher, Jr., "Median filters: some modifications and their properties", IEEE Trans.ASSP, ASSP-30, 739 (1982).

FIGURE CAPTIONS

1. (a) Optical setup for obtaining eigenvalues of circulant matrices.
   (b) Sketch of the matrix transparency.
   (c) Sketch of the focal plane light distribution.

2. Method for encoding complex matrices.

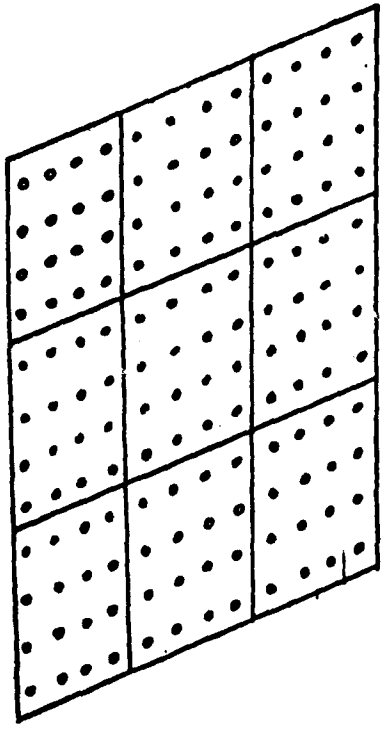

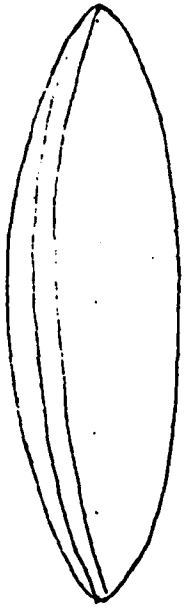

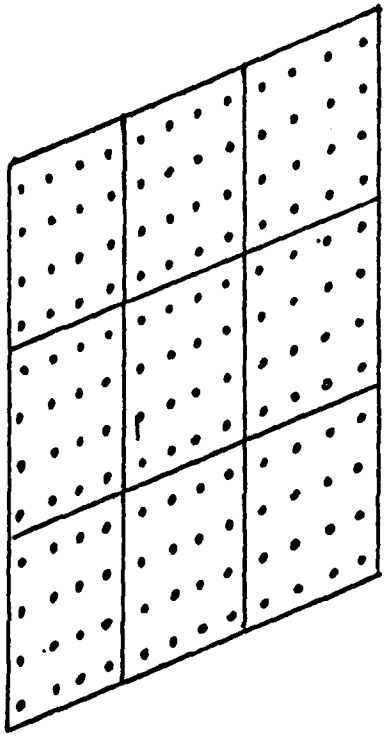

Sampled & Replicated object

Sampled & Replicated Spectrum

FIG. 1(a)

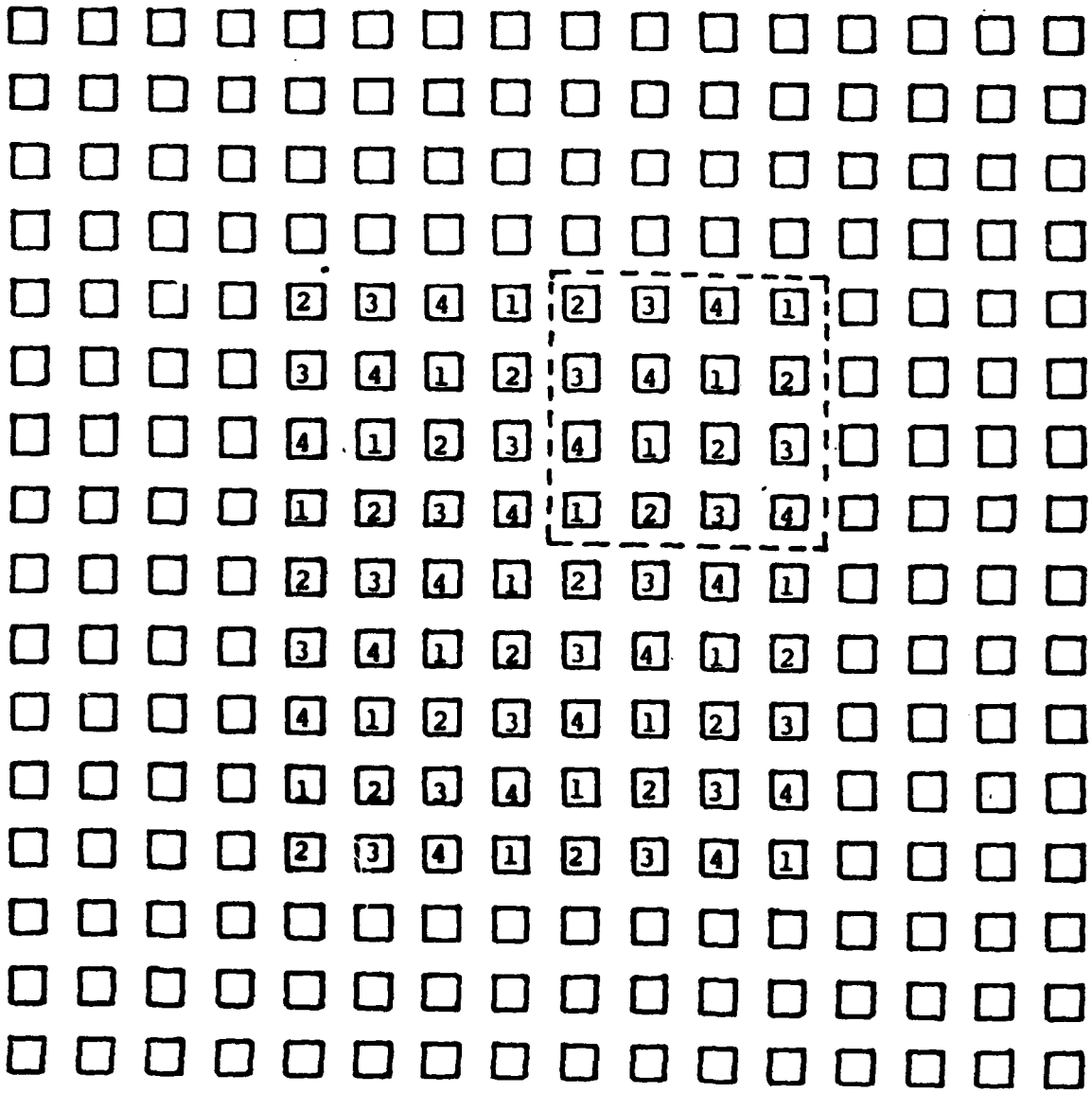

INPUT OF A 4X4 CIRULANT MATRIX

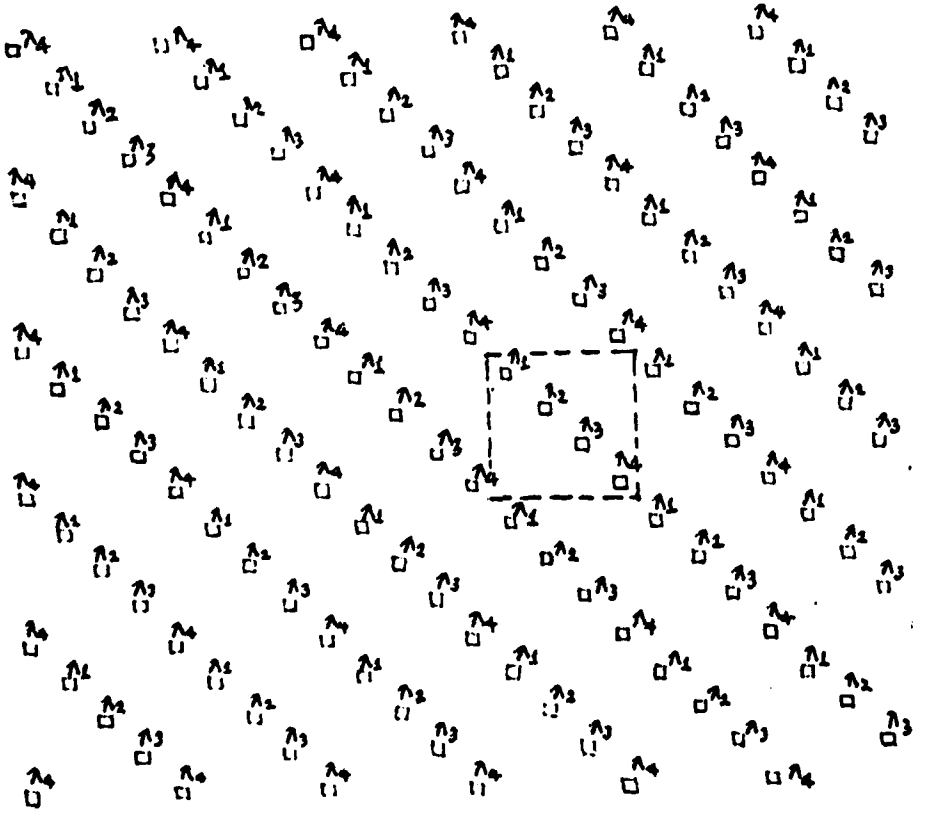

output for a 4x4 circulant matrix

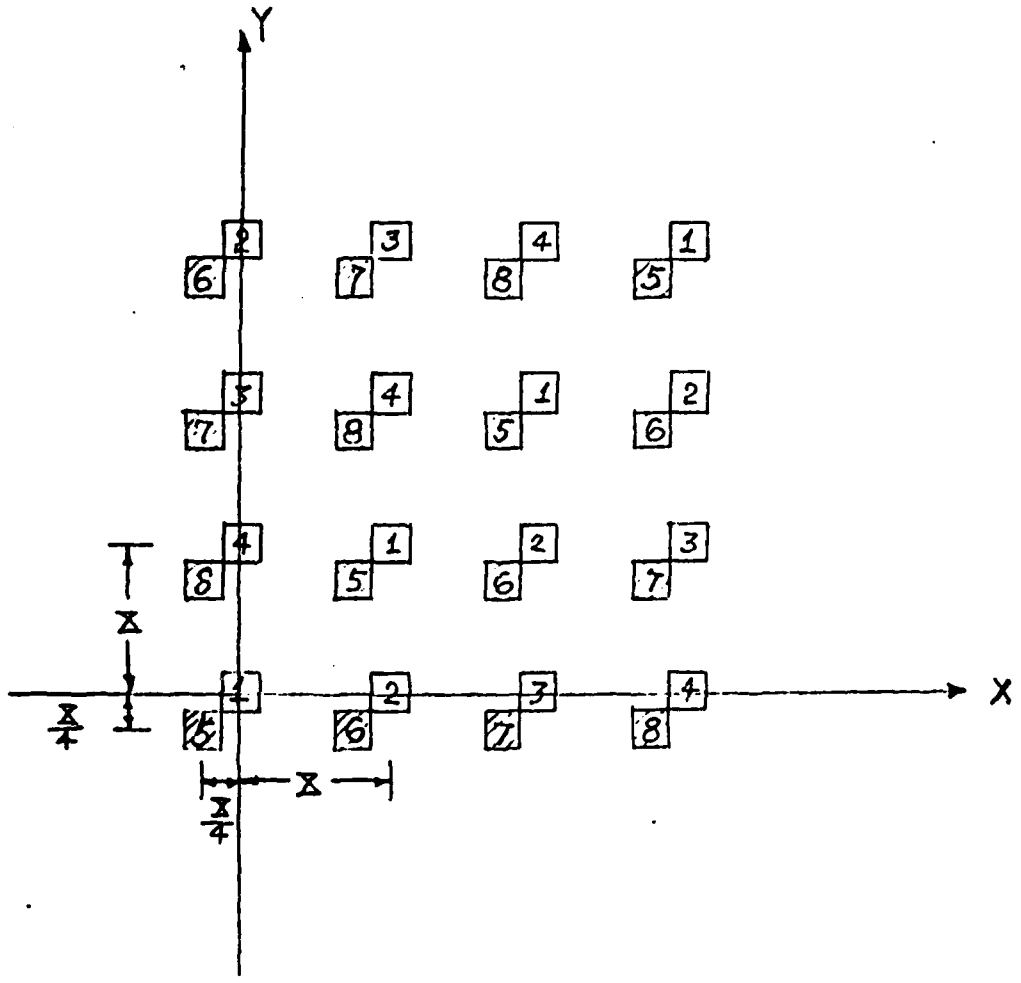

original Function —

$g(x,y) = R(x,y) + jI(x,y)$

□ — Real part

⬚ — Imaginary part

Input Function —

$g'(x,y) = R(x,y) + I(x+\frac{X}{4}, y+$

Complex number encoding

To

APPENDIX I

Architectural Development of Optical Data Processing Systems

J. W. GOODMAN

SUMMARY The architectural development of optical data processing systems is traced, beginning with the foundation established by Abbe and ending with a discussion of new trends. Some speculation on the future of the field is also included.

1 INTRODUCTION

The historical development of optical data processing architectures can be represented in the form of a tree. Like a tree, the field has roots, a strong trunk, major branches that subdivide into smaller limbs and new growth. In many cases the branches intertwine. In this paper we describe the major structures of this tree and speculate about future growth. The reader may wish to refer to fig. 1, showing the structure of this tree, as we proceed through the material that follows. The picture presented is a personal and subjective one, as it must be in any evaluation of past developments and speculation about the future yet to come.

2 THE ROOTS AND THE TRUNK

The lower roots of the optical data processing tree are undoubtedly the work of E. Abbe in the late 19th century [1]. Abbe recognised that coherent optical imaging systems accept and reject various grating structures associated with an object. He thereby introduced the notion that such systems act as spatial filters, although this term was not used. The upper roots of the tree are perhaps best attributed to F. Zernike, whose invention of the phase contrast microscope [2] provides the most remarkable early example of a successful attempt to manipulate the spatial spectrum of a coherent object for useful purposes.

The lower trunk of the tree is the work of Marechal [3], Tsujiuchi [4], O'Neill [5], Lohmann [6], and others, who were among the first to apply coherent optics to optical data processing problems, including image deblurring and extraction of two dimensional signals from noise. The upper trunk of the tree is the work of Cutrona, Leith, Palermo and Porcello [7] at the University of Michigan, who first emphasised the generality of optical processors and outlined a multitude of methods for putting such systems to use in the field of radar signal processing.

In the early 1960's the tree forked into several branches. We will trace the development of these branches in the following sections.

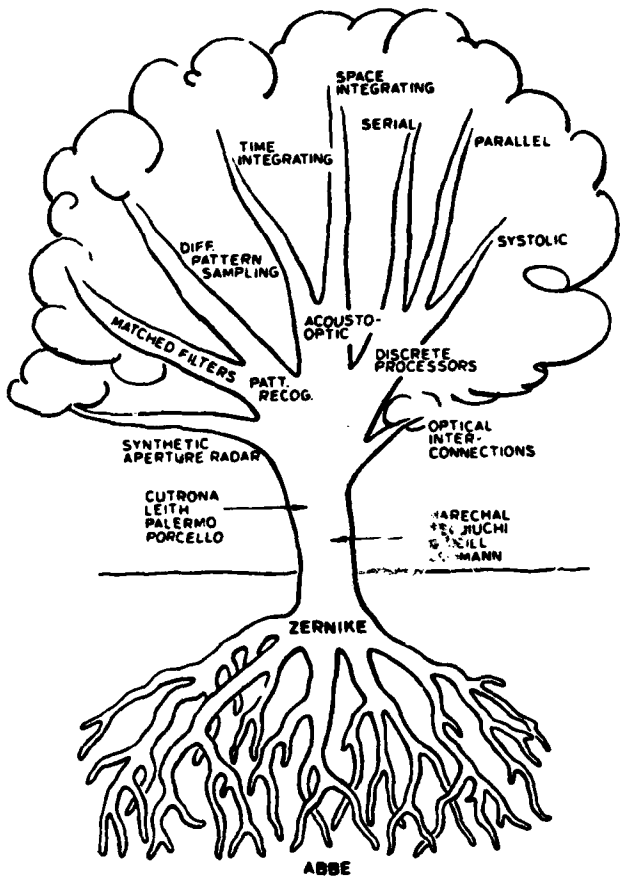

Figure 1 The tree describing architectures for optical data processing.

3 THE SYNTHETIC APERTURE RADAR BRANCH

One of the first and most important branches of the optical data processing tree is devoted entirely to the processing of signals collected by synthetic aperture radars.

As shown in fig. 2 (a), an aircraft carrying a radar transmitter and receiver flies a straight-line path over terrain of interest. Radar pulses are transmitted normal to the flight path and the returning

Invited paper submitted to The Institution of Radio and Electronics Engineers Australia on 30 March 1982.

echoes are mixed with a highly stable local oscillator in the radar receiver. A point scatterer on the ground returns a series of echoes as the aircraft flies past. Figure 2 (b) shows a typical record of the returned signal from two point scatterers at different ranges, as recorded in the aircraft. It is assumed that the radar transmits short pulses (although the use of longer "chirp" pulses is also permitted). Range information, plotted vertically, is obtained by pulse echo timing, while azimuth information, plotted horizontally, records the complex amplitudes of the fields received from scatterers at each range from the flight path. From this data it is desired to form an image of the terrain reflectivity. Note that the record from a single scatterer takes the form of a one-dimensional zone plate, with a focal length that depends on the distance of the scatter from the flight path.

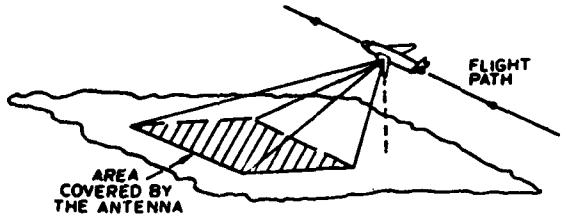

(a)

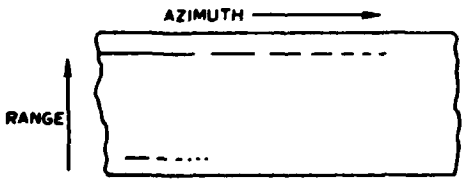

(b)

Figure 2 (a) Synthetic aperture radar data collection. (b) Record obtained for two scatterers.

When short pulses are used, the image in the range direction lies at the film on which the data was recorded. However, due to the dependence of the zone-plate focal lengths on range, the azimuth structure of the image lies in a tilted plane behind the film, as shown in fig. 3. The purpose of the optical processor is to bring the range and azimuth images into coincidence, as can be accomplished by means of an anamorphic optical system. An early version of such a processor [8] used a conical lens at the film plane to move the azimuth image to infinity, a cylindrical lens to the right of the film to move the range image to infinity and a spherical lens further to the right to bring the two infinitely distant images back to coincidence (see fig. 4). However, the image so-formed has a magnification that is range dependent and therefore an output slit was required. As the input data film and the output recording film are moved in synchronism, an image of the reflectivity of the terrain is recorded.

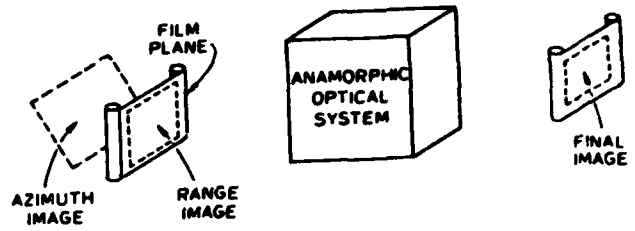

Figure 3 Range and azimuth image locations.

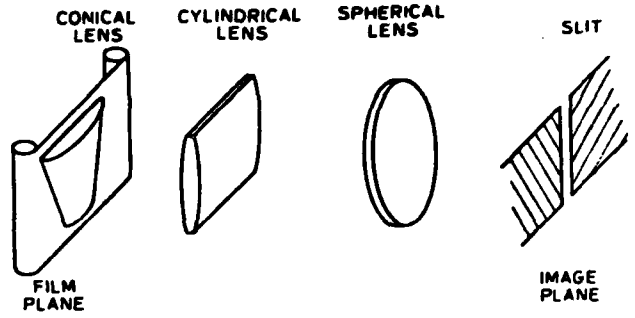

Figure 4 An early optical system for processig synthetic aperture radar data. Note the output slit.

An improved optical system, called the tilted plane processor, was described in 1972 by Kozma, Leith and Massey [9]. As shown in fig. 5, an anamorphic telescope system is used, together with a tilted input plane and a tilted output plane, to bring the range and azimuth images planes into coincidence with a magnification that is no longer range dependent. The need for the output slit is thus eliminated and significantly better processor performance is obtained.

The tilted plane processor remains today one of the most sophisticated processors in the entire field of optical data processing. It has demonstrated a continuing usefulness, even in the face of improved capability of digital processing systems.

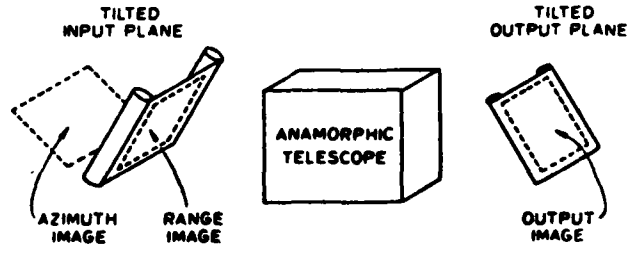

Figure 5 The tilted plane processor. Note the absence of an output slit.

4 THE OPTICAL PATTERN RECOGNITION BRANCH

A second major branch of the tree grew out of the potential application of coherent optical systems to pattern recognition problems. The origins of this branch lie in the work of Vander Lugt [10] in1964, who originated and demonstrated the first highly practical method for generating complex matched

filters for two-dimensional objects. The optical filtering system is the standard one shown in fig. 6, in which input is introduced by means of film or a real-time light valve, the first lens Fourier transforms the input fields, the filter placed in the focal plane modifies the Fourier spectrum of the object and the second lens inverse transforms the modified spectrum to produce a filtered output image. Vander Lugt's important contribution was the origination of the idea of an interferometrically recorded (or holographic) Fourier-plane filter, which could control the complex amplitude transmittance through the focal plane in an extremely flexible way. In particular, a filter can be generated that has as its amplitude transmittance the complex conjugate of the Fourier spectrum of an object from which the filter was made. Thus if a certain object $o(x,y)$ has as its Fourier spectrum the complex function $O(f_x,f_y)$, a filter with amplitude transmittance

$$t(x,y) = O^*(f_x,f_y) \qquad (1)$$

can be constructed. Such a filter is said to be "matched" to the object $o(x,y)$; it will produce a bright output spot of light at any position where the particular object $O(x,y)$ is present in the input field. The Vander Lugt filter has played an important role in the development of optical matched filtering approaches to pattern recognition.

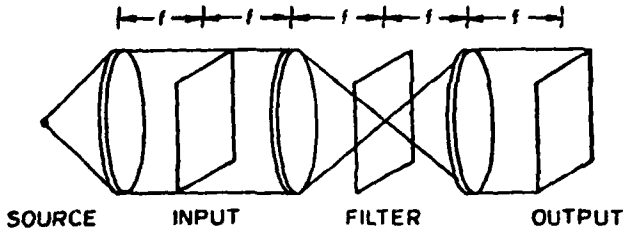

Figure 6 Standard coherent optical processing system.

While the idea of the interferometrically generated filter for matched filtering applications has had an extremely large intellectual impact, it must be said that after nearly 20 years of research the applications of such filters are disappointingly limited. The difficulties lie not with the concept of the interferometrically generated filter, but with the use of a matched filter. While the matched filter response is not affected by pure translation of the position of the object at the input (the output spot simply moves with the input), such filters are exceedingly sensitive to scale size and rotation of the object to be recognised. That is, if a matched filter is constructed for recognition of an object with one particular scale size and rotational orientation, the filter will usually produce very little response to that same object presented at the input with a different scale size or orientation.

Attempts to overcome this undesired sensitivity have been clever but not very successful. We mention in particular the elegant Mellin filtering approach of Casasent and Psaltis [11]. The input data is presented to the processor in polar coordinates, rather than rectangular coordinates. In addition, the axis corresponding to radial position is intentionally streched by a logarithmic spatial distortion. As a consequence, it can be shown that the Fourier transform of the radial structure of the image is identical with a so-called Mellin transform and the magnitude of the Mellin transform is invariant under changes of scale size (magnification of the input). Simultaneously the optical system Fourier transforms the angular structure of the input. With suitable care to take account of edge effects, rotation of the object is equivalent to translation in the angular direction. Since matched filters do respond properly to translated versions of the structures to which they are matched, the Mellin matched filter will respond properly to an input object regardless of its scale size or its angular rotation. Unfortunately the process of desensitising the system to magnification and rotation has introduced a sensitivity that was not present originally, namely to the position of the object in the input field. The Mellin matched filter will not respond properly to objects that have a different position in the input field than they had when the matched filter was constructed. Casasent and Psaltis [12] solved this problem by entering into the system only the *power spectrum* of the input pattern, a quantity that is independent of the position of that pattern. However, the discarding of all phase information in the amplitude spectrum results in a decrease in the ability to discriminate between different patterns. As a consequence the problem of simultaneous position-, size-, and rotation-invariant optical pattern recognition has not yet been solved in a fully satisfactory way.

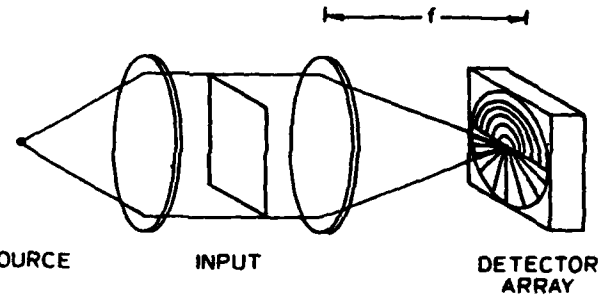

Figure 7 Diffraction pattern sampling system.

The "pattern recognition" branch has a sub-branch that is particularly worthy of mention. We refer to so-called "diffraction pattern sampling" systems which base pattern recognition decisions on the structure of the optically obtained Fourier transform of an input [13]. The system is illustrated in fig. 7. The input is presented to the system as a transparency. The coherent optical system Fourier transforms that input, displaying an intensity distribution across the back focal plane that is the power spectrum of the input. A detector consisting, for example, of combinations of rings and wedges, is used to extract a reduced amount of data from the power spectrum. The powers measured by these detector elements are then digitised and digital pattern recognition algorithms are applied to classify the input. This system has several properties that make it potentially very useful. First, the detector in the focal plane performs an all-important reduction of information, presenting the digital system with data of reduced complexity but still retaining sufficient information for the particular task at hand. Second, the system combines optical and digital computations in an appropriate way, with each system doing computations for which it is particularly well suited. In spite of the many nice features to recommend this approach to

this approach to pattern recognition, it has received less use than it deserves. Perhaps the increasing emphasis on robotics and computer vision will lead to a renewal of interest in the diffraction-pattern sampling approach.

5 THE ACOUSTO-OPTIC SIGNAL PROCESSING BRANCH

A third major branch of the optical data processing tree derives its strength from developments in acousto-optic device technology. The branch begins in the early 1960's with the work Rosenthal [14], Slobodin [15], and Arm, Lambert and Weissman [16] on the use of acousto-optic devices for signal processing. An excellent review of this area is found in reference 17 and accompanying papers in the same issue.

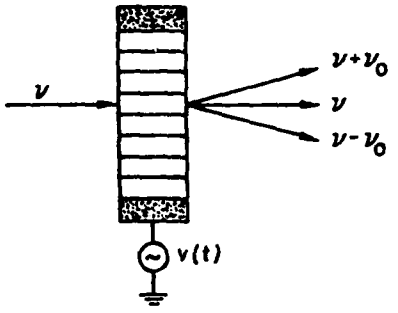

(a)

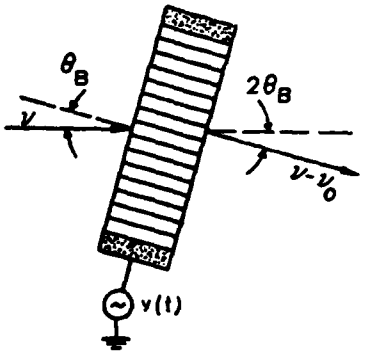

(b)

Figure 8 (a) Acousto-optic cell in the Raman-Nath regime. (b) Acousto-optic cell in the Bragg regime.

Before beginning a discussion of acousto-optic signal processing architectures, it is perhaps worthwhile to present a small amount of background on the acousto-optic devices themselves. Figure 8 illustrates acousto-optic cells in two different modes of operation. In both cases, an electrical signal v(t), consisting of an amplitude and phase modulated carrier,

$$v(t) = A(t)\cos[2\pi\nu_0 t + \phi(t)], \qquad (2)$$

is applied to an acousto-optic transducer, which launches an acoustic wave in the transparent medium of the cell. The presence of the acoustic signal results in local changes of the refractive index of the cell, with the result that an optical signal propagating across the sound beam experiences spatially varying phase modulation. Figure 8 (a) shows the so-called Raman-Nath regime of operation, in which the cell thickness and spatial period of the acoustic signal are such that the cell acts as a "thin" phase grating, generating a multitude of diffraction orders, each with a different propagation angle and a different optical frequency; only the zero and first order beams are shown. Figure 8 (b) shows the more common Bragg regime, in which the cell acts as a "thick" phase grating, with only one or two diffraction orders of significant intensity and requiring illumination of the cell at the Bragg angle in order to produce a strong component of diffracted light. Early attention to devices operating in the Raman-Nath regime soon turned to devices operating in the Bragg regime, where wider bandwidths can be achieved.

This acousto-optic signal processing branch has had remarkable growth in recent years. This growth has been caused partially by advances in the technology of acousto-optic cells and partially by development of new architectures in which such cells can be used. The branch can be said to have forked into two major sub-branches, space-integrating processors and time-intergrating processors. Each of these sub-branches has a complicated branching structure and the growth is so dense that the two are at least partially intertwined.

Most important in the space-integrating lineage is the Bragg-cell spectrum analyser, shown in fig. 9, which has enjoyed a success in application that is beginning to rival that of the tilted-plane processor mentioned earlier (although the applications are quite different). The Fourier transforming properties of coherent optical systems areused here to perform spectrum analysis of temporal signals, the temporal signals being introduced into the processor as spatial signals travelling through the input acousto-optic cell. Coherent optical spectrum analysers with approximately one Ghz of bandwidth and time-bandwidth products of approximately 1000 are now in use in a number of laboratories and the number of lower performance systems is even more plentiful. Integrated optic versions of such spectrum analysers are also being constructed, based on surface-acoustic-wave input of RF signals.

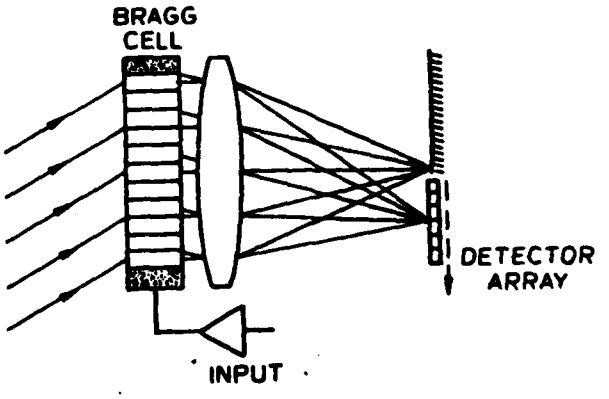

Figure 9 Bragg spectrum anaslyser.

A second architecture in this same space-integrating lineage is the space-integrating correlator, in which one or even two Bragg cells may be used to perform correlation of two signals. A typical

configuration is shown in fig. 10. The r.f. signal $v_1(t)$, having complex envelope

$$A(t) = |A(t)| \exp[j\phi(t)], \qquad (3)$$

where $A(t)$ and $\phi(t)$ are the amplitude and phase modulations of $v_1(t)$, is to be correlated with a second signal $v_2(x)$ (complex envelope $B(x)$) whichis stored as a fixed reference function on a mask. Using the optical system shown in the figure, the current generated by a point detector located on the optical axis in the output plane takes the form

$$i_d(t) = \left| \int_{-\infty}^{\infty} A^*(x-Vt)\, B(x)\, \mathrm{rect}(x/W)\, dx \right|^2 \qquad (4)$$

where V is the velocity of propagation of the acoustic wave in the input cell, W is the length of the illuminated region of the acoustic cell and rect(x) is defined to be unity for $-\frac{1}{2}<x<\frac{1}{2}$ and zero otherwise. As the name implies, the correlation integral is performed over space, while different values of delay are realised in time.

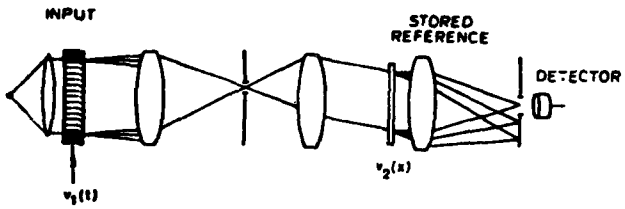

Figure 10 Space-integrating correlator.

The sub-branch representing time-integrating correlators begins in 1972 with the patent of R.M. Montgomery [18]. A more widely known developmentof these ideas is found in the work of Sprague and Koliopoulos [19] in 1976. This architecture, which is illustrated in fig. 11, uses integration in time for performing the correlation integral itself, while using space to represent various values of delay. One of the signals to be correlated, $v_1(t)$, is input as a traveling acoustic wave in the first cell, while the second signal is introduced as a counterpropagating wave in the second cell. The Bragg effect results in only a zero order and a negative first order being transmitted by the first cell, while each of these orders is split into a zero order and a negative first order by the second cell. The zero-order beams are both blocked. The first-order beams, which are at the same optical frequency, are both passed and are allowed to interfere on a time integrating detector array at the output. The spatial distribution of time integrated intensity takes the form

$$E_d(x) = \text{bias terms} + \mathrm{Re}\left\{ \int_T A^*(t-x/V)B(t+x/V)\, dt \right\} \qquad (5)$$

where T represents the total integration time (limited in practice by bias build-up). Note that for each different value of x, the integrated intensity is determined by the value of the cross-correlation function, evaluated at time delay $2x/V$.

The significance of the time-integration architecture is that the time-bandwidth product achieved is no longer constrained by the space-bandwidth product of the processor but rather is determined by the length of the time integration, which in turn is limited by the dynamic range of the detector. The space-bandwidth product of the processor limits the range of achievable delays for which the cross-correlation function can be measured.

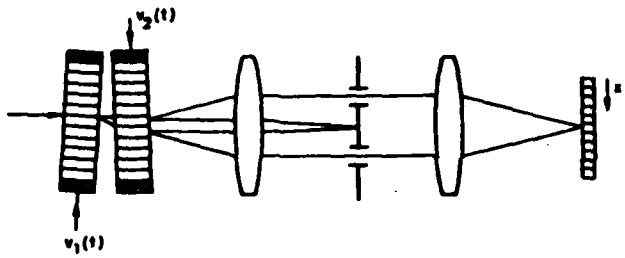

Figure 11 Time-integrating correlator.

An alternate form of the time-integrating correlator, as introduced by Kellman [20] and Turpin [21] is shown in fig. 12. In this case one of the signals is introduced as a time modulation of the intensity of an LED or laser diode source, while the second signal is introduced via an acousto-optic cell. The spatial filter shown in the focal plane of the second lens blocks all but the plus first and zero diffraction orders and shifts the phase of the zero order by 90 degrees with respect to the first order.

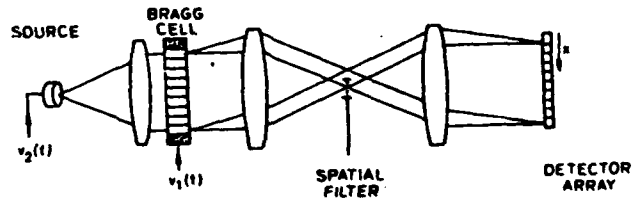

Figure 12 Time-integrating correlator with a modulated source.

A close relative of the time-integrating correlator is the triple product processor of Kellman [22], which allows the more general class of two-dimensional operations

$$E_d(x,y) = \text{bias terms} + \int_T v_1(t)\, v_2(t-x/V)\, v_3(t-y/V)\, dt \qquad (6)$$

to be performed.

The acousto-optic signal processing branch is an extremely healthy and vigorous one, with continued growth at the tips of the branches. There has recently been a tendency for the space-integrating and time-integrating branches to grow back together, with processors being proposed that use both types of integration simultaneously.

6 DISCRETE OPTICAL PROCESSORS

A relatively young vigorous branch of the architectural tree represents activities in the development of discrete optical processors. Such processors can perform the discrete analogs of any continuous-time

linear operations. The general type of operation performed is a matrix-vector product of the form

$$y = Ax$$

where x is a length M input column vector, A is an NxM matrix and y is a length N output column vector. It should be emphasised that, while the systems of concern are discrete (i.e., based on discrete mathematics), they are none-the-less analog systems and subject to the usual limitations on accuracy and dynamic range typical of such systems.

Early versions of optical matrix-vector multipliers were based on the use of coherent light [23-5]. Incoherent implementations were also devised [26,27].

However, a most significant advance in this area came from the work of Bocker [28], Bromley [29] and Monahan *et al* [30], who devised a method for matrix-vector multiplication using a single light-emitting diode (LED) source and a two dimensional charge-coupled-device (CCD) detector array, as illustrated in fig. 13. This development is represented by an entire sub-branch in our tree. In explaining the basic operation of such a system, we assume for the moment that all elements of the input vector x and the matrix A are non-negative and real, so that they can be represented by light intensities or intensity transmittances. The elements of the input vector x are entered into the system in time sequence as pulses with intensities proportional to the desired values. The light from each pulse diverges and falls on the entire matrix mask, which contains an array of cells with intensity transmittances proportional to the elements of the desired matrix. The light transmitted by the mask falls on the two-dimensional CCD detector. The clocking of the CCD device is such that charges accumulated in a given cell are transfered one column to the right (i.e., out of the paper in the figure) along a fixed row before the occurrence of the next optical pulse and in this way the contributions of all pulses are accumulated, row by row. For example, if the first pulse represents the vector element x_1, and $h_{k,1}$ represents the element of the matrix mask in the kth row and first column, the charge deposited in the kth detector element of the first column is proportional to

$$Q_k^{(1)} = h_{k,1}x_1.$$

This charge is clocked one column to the right and the second pulse, with intensity proportional to the vector element x_2 is emitted. In the second column and the kth row, the total accumulated charge becomes

$$Q_k^{(2)} = h_{k,1}x_1 + h_{k,2}x_2.$$

After M pulses and M charge transfers, the total charge accumulated in the kth element of the last column of the detector is

$$Q_k(M) = \sum_{p=0}^{M-1} h_{kp}x_p$$

which is precisely the kth element of the desired output vector y. In principle, all N elements of the output vector are available in parallel but only after M cycles of the clock.

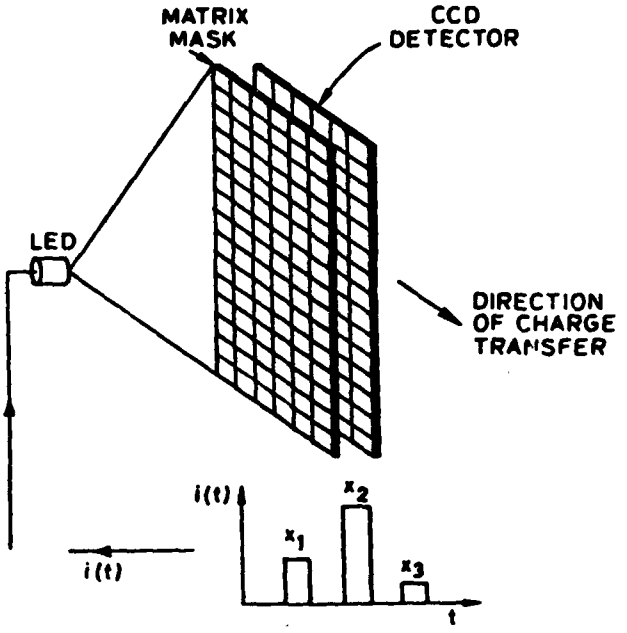

Figure 13 Serial incoherent matrix-vector multiplier.

A system of the type described above is capable of multiplying a matrix of approximately 500 x 500 elements times a 500-length vector of non-negative and real elements with clock rates of approximately 10MHz.

Incoherent systems of this kind are not restricted to performing operations involving only non-negative and real quantities. It is possible to code any bipolar real quantity and indeed any complex-valued quantity in terms of two nonnegative and real quantities, although in the latter case certain bias terms must be subtracted from the computed result [31]. We do not dwell on the details here, it being sufficient to say that fully complex operations can be performed at the price of doubling the size of the matrix and the length of the vectors.

A second sub-branch of the branch of discrete optical processors is represented by a closely related but faster incoherent discrete system introduced by Goodman, Dias and Woody [32] in 1978. In this case, as illustrated in fig. 14, the elements of the input vector are introduced in parallel on an array of LED's and the elements of the output vector are detected in parallel on an array of independent detector elements. The first box labeled "optics" spreads the light from each LED into a vertical column, which illuminates a single column of the matrix mask. The second box labeled "optics" places on each photodetector a light intensity proportional to the sum of the light intensities transmitted by an entire row of the matrix mask. These two operations result in detected signals proportional to the desired elements of the output vector y. Versions of this system based on discrete optical components (i.e., anamorphic systems of lenses) and multi-mode optical waveguides have been built [33]. The chief disadvantages of the system are the relatively short lengths of the vectors that can be accommodated and the absence of any data compression or information reduction in the operations performed. The latter fact results in exceedingly high rates with which data pours out of the system (potentially as high

as 10 GHz or more for a 100-channel system).

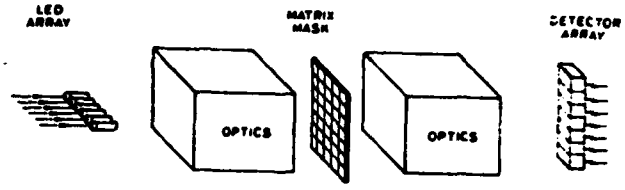

Figure 14 *Parallel incoherent matrix-vector* multiplier.

An exceedingly interesting development, constituting an extension of the sub-branch discussed above, is the use of the parallel incoherent matrix-vector multiplier in an iterative mode as a means for *solving simultaneous sets of linear equations* [34]. In this case we are given a set of simultaneous linear equations of the form

$$Mx = c$$

where M is a known matrix and c is a known vector and our goal is to determine the elements of the unknown vector x. A feedback arrangement as illustrated in fig. 15 can be shown to result ideally, after a sufficient number of iterations, in convergence of the output vector to the desired solution x. This innovation is significant for optical data processing for the following reason. Nearly all previous uses of optical processing have been for performing operations such as convolutions, correlations and Fourier transforms, where the number of elementary operations required is of order N^2 (N being the number of degrees of freedom of the input) but for which fast algorithms exist reducing the required number of operations for a digital implementation to order NlogN. The problem of solving a set of N simultaneous linear equations for the values of N unknowns is fundamentally an operation requiring order N^3 operations and, in the general case, no fast algorithms exist. Any application of optical processing to the domain requiring N^3 operations has potentially great rewards, for in such cases the "crutch" of fast algorithms is no longer available to the digital hardware that competes with the optical processor and the inherent speed and parallelism of the optical approach has its greatest significance.

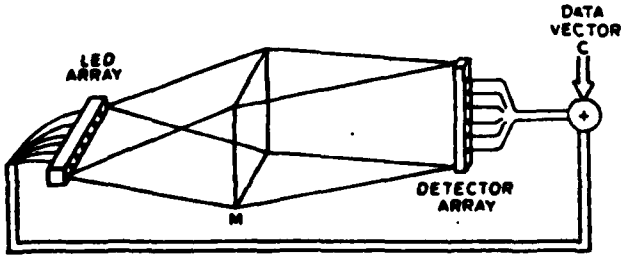

Figure 15 Incoherent matrix-vector multiplier with feedback.

The area of iterative optical processing remains an active one, with considerable potential for useful contributions. Recently optical implementations of iterative methods for finding the eigenvalues and eigenvectors of matrices have been proposed [35, 36] and no doubt other clever applications of this type of processor will be found in the future. However, such processors have not yet been fully analysed from the point of view of accuracy and numerical stability. The chief disadvantage of optical processors in these applications is clearly the limited accuracy associated with any analog approach to computation. This disadvantage will undoubtedly limit the kinds of matrices that can be successfully dealt with in this fashion [37].

The last sub-branch from the discrete optical branch is one we will call "systolic processors". This *sub-branch is exceedingly young and immature* but also exceedingly interesting as a novel approach to optical computation. The only published works on optical systolic processors at the time of this writing are those of Caulfield, Rhodes, Foster and Horvitz [38] and Casasent [39].

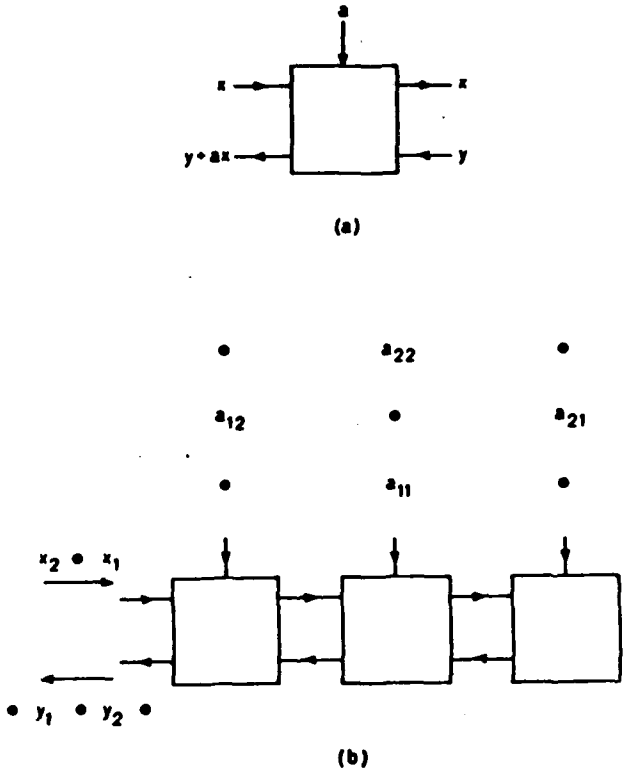

Figure 16 (a) Basic building block of a systolic processor. (b) Three processors interconnected in a systolic array.

The systolic processor architecture is the invention of H. T. Kung and C. E. Leiserson [40] and has been considered primarily as an architecture for VLSI implementation. There are in fact many different architectures for systolic processors, depending on the operation to be performed. We consider here only the simplest of these, namely one designed to perform the matrix-vector product discussed earlier. The basic building block of the systolic processor is illustrated in fig. 16(a). An input x, representing one element of the input vector, arrives from the left. Simultaneously a weighting coefficient a, representing an element of the matrix A, arrives from above. The processor, represented by the box, receives the input x from the left and passes it unchanged to the right along the upper

input line; simultaneously it accepts the value y coming from the right on the output line and transforms it into the new value y+ax, which continues to pass to the left.

Figure 16(b) shows three basic processors connected together in a structure that will multiply a 2x2 matrix A times a length 2 input vector x, producing a length 2 output vector y. We can regard this structure as being a pair of coupled delay lines in which input and output signals counter-propagate and with coupling coefficients that depend on the elements of the matrix A. The elements of the matrix are displayed above the processors and are assumed to arrive with a timing represented by their vertical distance above the processors. Any time interval represented by a dot in this diagram contains a coupling coefficient that is immaterial, since it will not affect the output signals of interest. The input data is entered from the left as a series of values, one every two cycles. The first input vector element, x_1, passes through the first processor, generating an output propagating to the left on the output line. This value is not of interest and is ignored. The input element then passes to the second processor, arriving coincident with the arrival of coupling coefficient a_{11}. The result is an output value $a_{11}x_1$ propagating to the left on the output line. This value arrives at the processor on the far left at the end of one cycle period. Meanwhile, a second input element x_2 has been launched on the input line and arrives at the first processor simultaneously with the arrival of the above partial output. The coupling coefficient at the first processor is a_{12}, resulting in a signal at the final output on the left of

$$y_1 = a_{11}x_1 + a_{12}x_2$$

In a similar way, the various coupled inputs yield a second output signal of the form

$$y_2 = a_{21}x_1 + a_{22}x_2,$$

i.e., the second element of the output vector y. The concept can clearly be extended to larger matrices and vectors.

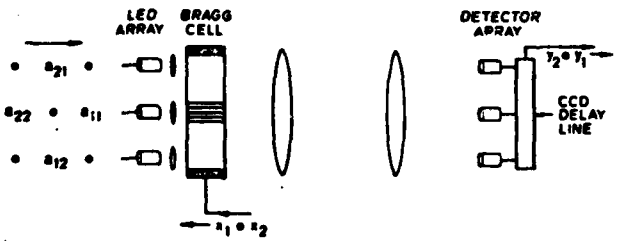

Figure 17 Optical systolic matrix-vector multiplier.

An optical analog version of the systolic matrix-vector multiplier has been proposed in reference 38 and is illustrated in fig. 17, again for the simple case of a 2x2 matrix. The elements of the input vector are entered as propogating pulses of short duration in an acousto-optic cell. The matrix elements are input in proper time sequence as intensity modulations of LED's in a parallel array. The output elements accumulate as moving charge packets on a clocked CCD device, fed by signals from a parallel array of detectors. The two delay lines involved are the acousto-optic cell (input) and the CCD device (output), with the coupling supplied by the strobed LED sources.

Another version of an optical systolic processor is under construction at Stanford University [41]. The processor, which we call a *fibre-optic scattering processor*, is illustrated in fig. 18. It consists of two single-mode optical fibres weakly coupled by a series of fibre-optic couplers. Ideally the couplers should be changeable with time but, as described shortly, useful signal processing operations can be performed even with fixed couplers. The elements of the input vector are entered as pulses of varying intensities on the input fibre, while the output elements accumulate as they propagate along the output fibre and emerge in time sequence. If the couplers have fixed coupling coefficients, rather than being time changeable, the structure of the matrix A is effectively constrained to be of Toeplitz form, i.e., the elements along any one subdiagonal are all identical. Such forms occur when the matrix-vector operation represents a convolution or a correlation, rather than a more general time-variant operation.

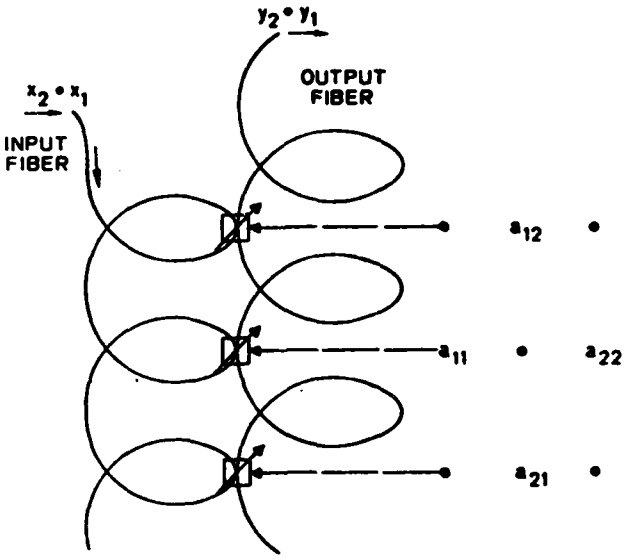

Figure 18 The fibre optic scattering processor.

It is difficult to avoid the feeling that these new architectures are but the beginning of a branch that will soon be developing a complicated network of offshoots, most of which are impossible to fully visualise or imagine at this particular point intime.

7 SOME SPECULATION ABOUT THE FUTURE

We have surveyed the past and present architectures of optical data processing systems. Perhaps in closing we will be permitted to speculate a bit about the future.

A reasonable starting point for this speculation is consideration of the weak and strong points of optical processors. A chief weakness of such data processing systems is, in our view, their inherent lack of accuracy, arising from the fact that they are purely analog in nature. A further weakness is the limited number of different types of basic operations such systems can perform, generally additions, subtractions, and multiplications. The

redeeming features of the optical processor is the speed with which computations can be performed in a highly parallel fashion.

By comparison, digital electronic processors can achieve accuracies limited only by the number of bits retained in the computation. In addition, their repertoire of types of basic operations is nearly unlimited.

The speed advantage associated with optics needs closer examination. The input and output devices used with such systems are usually electronic in nature and therefore there is generally an electronic bottleneck, limiting the rate at which data can enter and exit the system. These electronic bottlenecks are partially compensated for by the parallelism with which the analog computations are performed within the processor. The root of this inherent parallelism lies in the relative ease with which optical signals can be used to provide multiple independent paths between different computational components of the processor (e.g., transparencies and lenses). Thus the strength of optics lies in its ability to provide *interconnections* of an extremely complex type between different computational elements, while the strength of digital electronics lies in the ability of its computational elements to provide flexible operations with high accuracy.

The question now quite naturally arises as to whether it might be possible to combine the good features of optics and electronics in a single processor. We suggest that the answer in the future will be affirmative. We envision a processor that is basically an electronic chip or a series of chips, with digital electronic computational elements but with interconnections between elements and/or between chips provided by optics. While the idea of using optical waveguides on a chip may have merit in some situations, it is our view that there is too little difference between metallic interconnections and waveguides for this change to be of paramount significance. Rather we would speculate that *imaging* interconnections are worthy of consideration. To illustrate what we mean by this term, consider the geometry shown in fig. 19(a), in which two chips are communicating by means of imaging interconnections. At various points on the chip on the left, computations have been completed and are ready for transfer to various points on the chip on the right. The chip on the left is assumed to contain several tiny sources of light or, in the case of light supplied from off the chip, several tiny modulators. The chip on the left is assumed to contain several detectors at different locations. Each source (or modulator) on the left is then imaged onto an appropriate set of detectors on the right. The imaging element is certainly more complicated than a simple lens. It might be a holographic optical element.

Of the many problems with the above idea that come to mind, chief among these is perhaps the fact that we do not know how to integrate optical sources on silicon. As indicated, however, it is not actually necessary to have sources on the chip, only modulators that can modify externally supplied light. Nonetheless, these modulators must be exceedingly small in size and capable of high-speed operation with very small power dissipation.

The ideas presented above can be extended to the case of a single chip as shown in fig. 19(b). In this case the holographic imaging element is reflective and resides above the chip.

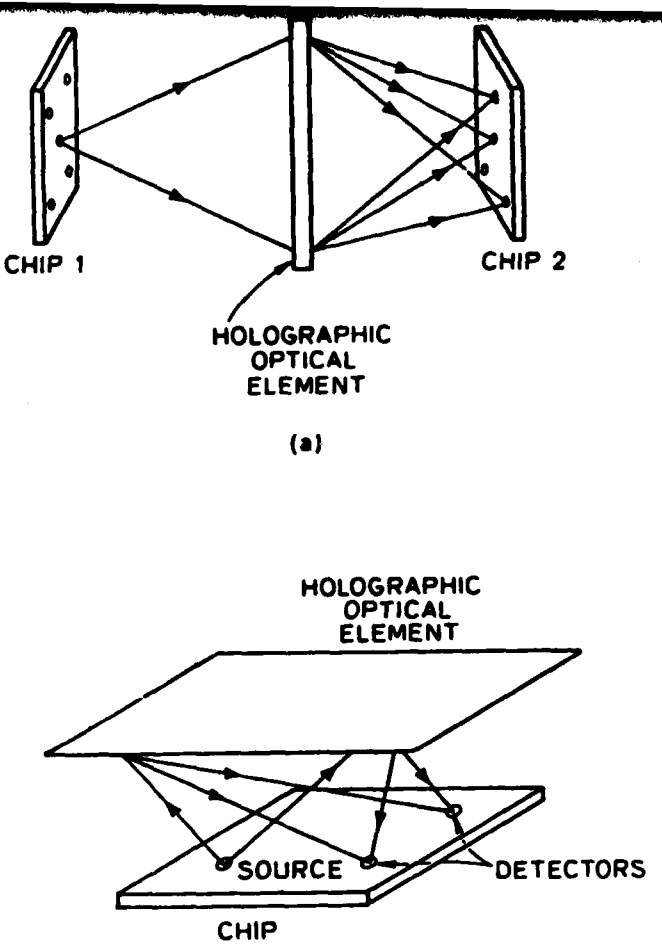

Figure 19 (a) Imaging interconnections between two chips by means of a holographic optical element. (b) Imaging interconnections within a single chip.

While the possibility of having sources or modulators on the chip may seem remote at this point in time, there is a subset of problems for which they are not needed in integrated form. This subset consists of data processing problems requiring enormous amounts of parallel data input to the processor but comparatively little data flow out. An excellent example of this type of processor is the systolic array described in the previous section. Let the input and output vectors be of length N, and the matrix be NxN. The elements of the input vector can be entered over a serial electronic communication line and likewise the elements of the output vector can leave the chip via a single serial communication line. However, the (2N-1) processors must receive an average of N different matrix elements every clock cycle, thus requiring either an enormous number of parallel input channels or a large degree of multiplexing, which will slow down the speed of operation. To provide parallel electronic input channels requires that the chip have a very large number of pins. This rather severe price can be avoided if data is input via a corresponding number of imaging optical interconnections, as shown in fig. 20. It is only necessary to integrate detectors on the chip. The need for a large number of bonding pads is elimin-

ated. While parallel electronics are needed to drive the light sources that are imaged onto the chip, such electronics can be relatively macroscopic in size, free from the constraints present in a single-chip environment. The prime computational elements of the architecture remain in the single chip environment, as needed for high speed and low power dissipation.

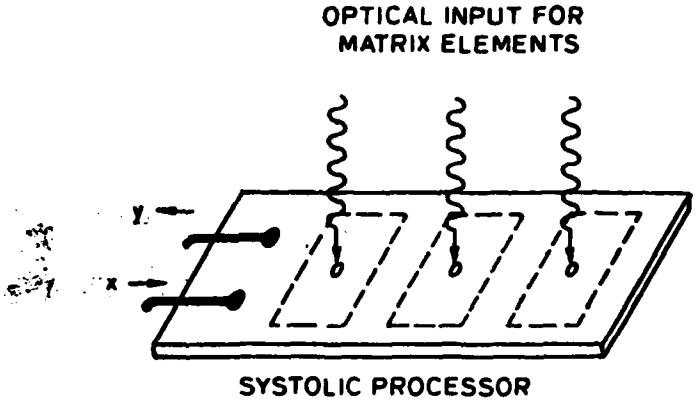

Figure 20 Replacement of pins by imaging optical connections.

The above ideas are clearly speculative but they do provide one possible scenario for future directions in optical data processing. Here it is no longer optics that does the actual computing but the role of optics as a means for interconnections is no less important than that of the digital electronic processors that perform the numerical computations.

8 ACKNOWLEDGMENTS

Support of the Air Force Office of Scientific Research is gratefully acknowledged.

9 REFERENCES

1. Abbe, E., "Beitrage zur Theorie des Mikroskops und der Mikroskpischen Wahrnehmung", Archiv. Mikroskopische Anat., Vol. 9, 1893, pp. 413-68.

2. Zernike, F., "Das Phasenkontrastverfahren bei der Mikroscopischen Beobachtung", Z. Tech. Phys., Vol. 16, 1935, pp. 454.

3. Marechal, A. and Croce, P., "Un Filtre de Frequences Spatiales pour l'Amelioration du Contrast des Images Optiques", C. R. Acad. Sci., Vol. 127, 1953, pp. 607.

4. Tsujiuchi, J., "Correction of Optical Images by Compensation of Aberrations and by Spatial Filtering", "Progress in Optics", Vol. II, (E. Wolf, Ed.), North Holland Publishing Co., Amsterdam, (1962), pp. 133-80.

5. O'Neill, E.L., "Spatial Filtering in Optics", Trans. IRE, Vol. IT-2, 1956, pp. 56-65.

6. Lohmann, A., "Optical Single-sideband Transmission Applied to the Gabor Miscroscope", Opt. Acta, Vol. 3, 1956, pp. 97-9.

7. Cutrona, L.J., Leith, E.N., Palermo, C.J. and Porcello, L.J., "Optical Data Processing and Filtering Systems", Trans. IRE, Vol. IT-6, 1960, pp. 386-400.

8. Cutrona, L.J., Leith, E.N., Porcello, L.J. and Vivian, W.E., "On the Appliction of Coherent Optical Processing Techniques to Synthetic-Aperture Radar", Proc. IEEE, Vol. 54, 1966, pp. 1026-32.

9. Kozma, A., Leith, E.N. and Massey, N.G., "Tilted Plane Optical Processor", Applied Optics, Vol. 11, 1972, pp. 1766-77.

10. Van der Lugt, A.B., "Signal Detection by Complex Spatial Filtering", Trans. IEEE, Vol. IT-10, 1964, pp. 139-45.

11. Casasent D. and Psaltis, D., "New Optical Transforms for Pattern Recognition", Proc. IEEE, Vol. 65, 1977, pp. 770-84.

12. Casasent, D. and Psaltis, D., "Position Rotation and Scale Invariant Optical Correlation", Applied Optics, Vol. 15, 1976, pp. 1795-9.

13. Thompson, B.J., "Hybrid Processing Systems - An Assessment", Proc. IEEE, Vol. 65, 1977, pp. 62-76.

14. Rosenthal, A.H., "Application of Ultrasonic Light Modulation to Signal Recording, Display, Analysis, and Communications", Trans. IRE, Vol. UE-8, 1961, pp. 1-5.

15. Slobodin, L., "Optical Correlation Technique", Proc. IEEE, Vol. 51, 1963, pp. 1782.

16. Arm, M., Lambert, L. and Weissman, I., "Optical Correlation Technique for Radar Pulse Compression", Proc. IEEE, Vol. 52, 1964, pp. 842.

17. Rhodes, W.T., "Acousto-optic Signal Processing: Convolution and Correlation", Proc. IEEE, Vol. 69, 1981, pp. 65-79.

18. Montgomery, R.M., "Acousto-optical Signal Processing System", U.S. Patent 3 634 749, January 1972.

19. Sprague, R.A. and Koliopoulis, C.L., "Time Integrating Acousto-optic Correlator", Applied Optics, Vol. 15, 1975, pp. 89-92.

20. Kellman, P., "Detector Integration Acousto-optic Signal Processing", Proc. 1978 Int. Optical Computing Conf., (Digest of Papers), IEEE No. 78CH-1395-2C, (1978), pp. 91-95.

21. Turpin, T.M., "Time Integrating Optical Processors", in "Real time signal processing", (F. Tao, Ed.), Proc. SPIE, Vol. 154, 1978, pp. 196-203.

22. Kellman, P., "Time Integrating Optical Signal Processing", Ph.D. Dissertation, Dept. Electrical Engineering, Stanford University, Stanford, California, June 1979.

23. Heinz, R.A., Artman, J.O. and Lee, S.H., "Matrix Multiplication by Optical Methods", Applied Optics, Vol. 9, 1970, pp. 2161-8.

24. Jablonowski, D.P., Heinz, R.A. and Artman, J.O., "Matrix Multiplication by Optical Methods: Experimental Vertification", Applied Optics, Vol. 11, 1972, pp. 174-8.

25. Tamura, P.N. and Wyant, J.C., "Matrix Multi-

plication Using Coherent Optical Techniques", in "Optical Information Processing", (D. Casasent and A.A. Sawchuck, Eds.), Proc. SPIE, Vol. 83, 1977.

26. Schneider, W. and Fink, W., "Incoherent Optical Matrix Multiplication", Optica Acta, Vol. 22, 1975, pp. 879-88.

27. Krivenkov, B.E., Mikhlyaev, S.V., Tverdokhleb, P.E. and Chugui, Y., "Non-coherent Optical Processing System for Processing of Images and Signals", in "Optical Information Processing", (Y.E. Nesterikhin, G.W. Stroke and W.E. Kock, Eds.), Plenum Press, New York (1976), pp. 203-17.

28. Bocker, R.P., "Matrix Multiplication Using Incoherent Optical Techniques", Applied Optics, Vol. 13, 1974, pp. 1670-6.

29. Bromley, K., "An Incoherent Optical Correlator", Optica Acta, Vol. 21, 1974, pp. 35-41.

30. Monahan, M.A., Bromley, K. and Bocker, R.P., "Incoherent Optical Correlators", Proc. IEEE, Vol. 65, 1977, pp. 121-9.

31. Goodman, J.W., Dias, A.R., Woody, L.M. and Erickson, J., "Some New Methods for Processing Electronic Image Data Using Incoherent Light", in "Optica Hoy y Manana", Proc. of ICO-11, (J. Bescos, A. Hidalgo, L. Plaza and J. Santamaria, Eds.), Sociedad Espanola de Optica, Madrid, Spain, (1978), pp. 139-45.

32. Goodman, J.W., Dias, A.R. and Woody, L.M., "Fully Parallel, High-speed Incoherent Optical Method for Performing Discrete Fourier Transforms", Optics Letters, Vol. 2, 1978, pp. 1-3.

33. Dias, A.R., "Incoherent Optical Matrix-vector Multiplication for High-speed Data Processing", Ph.D. Dissertation, Dept. of Electrical Engineering, Stanford University, Stanford, California, 1980.

34. Psaltis, D., Casasent, D. and Carlotto, M., "Iterative Color-multiplexed Electro-optical Processor", Optics Letters, Vol. 4, 1979, pp. 348-50.

35. Caulfield, H.J., Dvore, D., Goodman, J.W. and Rhodes, W.T., "Eigenvector Determination by Noncoherent Optical Methods", Applied Optics, Vol. 20, 1981, pp. 2263-5.

36. Kumar, B. and Casasent, D., "Eigenvector Determination by Iterative Optical Methods", Applied Optics, Vol. 20, 1981, pp. 3707-11.

37. Goodman, J.W. and Song, M., "Performance Limitations of an Analog Method for Solving Simultaneous Linear Equations", Applied Optics, Vol. 21, 1982, pp. 502-6.

38. Caulfield, H.J., Rhodes, W.T., Foster, M.J. and Horvitz, S., "Optical Implementation of Systolic Array Processing", Optics Communications, Vol. 40, 1982, pp. 86-90.

39. Casasent, D., "Acoustooptic Transducers in Iterative Optical Matrix-vector Processors", Applied Optics, Vol. 21, 1982, pp. 1859-65.

40. Kung, H.T. and Leiserson, C.E., "Algorithms for VLSI Processors", in "Introduction to VLSI", C.A. Mead and L.A. Conway, AddisonWesley, Reading, Mass. (1980), pp. 271.

41. Tur, M., Goodman, J.W., Moslehi, B., Bowers, J.E. and Shaw, H.J., "Fibre-optic Signal Processor with Applications to Matrix-vector Multiplication and Lattice Filtering", accepted for publication in Optics Letters.

DR. J.W. GOODMAN

Joseph W. Goodman received the A.B. Degree in Engineering and Applied Physics from Harvard University in 1958, and the M.S. and Ph.D. degrees in Electrical Engineering from Stanford University in 1960 and 1963, respectively.

From 1958 through 1962, he was a Research Assistant in the Stanford Electronics Laboratories. During 1962 and 1963, he was a post-doctoral Fellow at the Norwegian Defense Research Establishment, under the auspices of the Royal Norwegian Society for Scientific and Industrial Research. He returned to Stanford in 1963 as a Research Associate, a position he held until 1967. In 1967 he was appointed Assistant Professor of Electrical Engineering at Stanford. He was promoted to Associate Professor in 1969 and to Professor in 1972, the position he now holds. During the academic year 1973-1974 he was a Visiting Professor at the Institute d'Optique, Orsay, France. Since January 1981 he has served as the Director of the Information Systems Laboratory at Stanford University.

Dr. Goodman has held positions of responsibility in the Optical Society of America, in the Society of Photo-Optical Instrumentation Engineers, and in the Institute of Electrical and Electronics Engineers.

His international activities include membership of the U.S. delegations to US-Japan, US-USSR, and US-Argentia Seminars on optical data processing. Dr. Goodman is a Fellow of the OSA, the IEEE, and the SPIE. In 1971 he was chosen recipient of the F.E. Terman award of the American Association for Engineering Education. He is the Author of approximately 100 technical publications, including the textbook "Introduction to Fourier Optics".

Mailing address: c/o Information Systems Laboratory, Department of Electrical Engineering, Stanford University, Durand Bldg. 127, Stanford, CA 94305, U.S.A.

Statistical Properties of Ray Directions in a Monochromatic Speckle Pattern

Ellen Ochoa
Joseph W. Goodman

Information Systems Laboratory
Department of Electrical Engineering
Stanford University
Stanford, California 94305

ABSTRACT

The statistical properties of the spatial derivatives of the phase of a monochromatic speckle pattern are studied. Initially, a one-dimensional probability density function for the derivative of the phase is obtained and compared to the solution for the analogous problem concerning instantaneous frequency of narrowband Gaussian noise. Subsequently, a two-dimensional probability density function is derived which depends on the two first and three second spatial moments of the illumination intensity distribution of the scattering object. Some sample intensity distributions are considered for which explicit expressions for the probability density function are given.

APPENDIX II

Statistical Properties of Ray Directions in a Monochromatic Speckle Pattern

Ellen Ochoa
Joseph W. Goodman

Information Systems Laboratory
Department of Electrical Engineering
Stanford University
Stanford, California 94305

Introduction

Speckle patterns arise when highly coherent light is transmitted through, or reflected from, an object with a surface that is rough on the scale of a wavelength. It has been found fruitful to treat the fields present in such a pattern as a random process, the randomness being over an ensemble of macroscopically similar but microscopically different rough surfaces. In this paper we are concerned with a very specific statistical property of such patterns, namely the statistical distribution of geometrical ray directions contained in the scattered fields. Equivalently, we are interested in the joint probability density function of the two components of the gradient of the phase distribution in a speckle pattern.

The statistical distribution of ray directions is of interest in a number of practical problems. For example, when a hologram is formed by interference of a plane reference wave and a wave generated by a diffuse object, knowledge of the statistical distribution of phase slopes allows specification of the statistical distribution of local spatial frequencies on the recording medium. If the hologram is thick, then this information also allows specification of the local tilt of the fringes within the emulsion, a quantity that influences the average diffraction efficiency that can be obtained. Finally, the results may be of interest in the field of adaptive optics, since many wavefront sensors measure the gradient of the phase of the incoming wave.

To our knowledge, the statistics of ray directions in speckle patterns have not been discussed in the literature before. Neither of the two general surveys of this field discusses the problem [1, 2]. The most closely related works are those of Ebeling [3] , who investigated the

statistical properties of the spatial derivative (along one arbitrary direction) of the amplitude and intensity in a speckle pattern, and Ohtsubo [4] , who studied the zero-crossing rate of the derivative of the intensity of a speckle pattern. Also worth mention are the classic works of Longuet-Higgins [5] , who studied the statistical properties of the derivatives of wavefronts with Gaussian phase deformations but constant intensities. Our problem is significantly different in that both the intensity and the phase are random, and the phase statistics are not Gaussian. Finally, we should mention that our problem has an exact one-dimensional analog that has been studied by communication theorists, namely the statistical distribution of the instantaneous frequency of narrowband Gaussian noise (see, for example, reference [6]). While the methods of solution of the one- and two-dimensional problems are similar, the two-dimensional solution is more complex, and the solution in two dimensions cannot be deduced simply from knowledge of the result in one dimension.

Background

A monochromatic speckle pattern can be described as a sum of contributions from N independently-phased, coherent radiators. A single component of one polarization component of the electric field E at time t has the form

$$E(x,y,z,t)=\frac{1}{\sqrt{N}}\sum_{k=1}^{N}|a_k|\,e^{i\phi_k}e^{i(\omega t+\theta)} \tag{1}$$

where $|a_k|$ and ϕ_k are the amplitude and phase of the kth radiator and are functions of x, y, and z. θ represents the initial phase and is a random variable uniformly distributed from $-\pi$ to π. Separating E into real and imaginary parts, we have

$$\begin{aligned} E(x,y,z,t) &= r + i \qquad (2)\\ &= \frac{1}{\sqrt{N}}\sum_{k=1}^{N}|a_k|\,[(\cos\phi_k\cos(\omega t+\theta)-\sin\phi_k\sin(\omega t+\theta)) + i(\cos\phi_k\sin(\omega t+\theta)+\sin\phi_k\cos(\omega t+\theta))]\\ &= |a|\,[\cos(\omega t+\phi) + i\sin(\omega t+\phi)] \end{aligned}$$

where ϕ is the phase of the resultant wave. Statistical properties of speckle are studied using the following assumptions:

(1) $|a_k|$, ϕ_k are statistically independent of each other and of all other $|a_j|, \phi_j$, for $j \neq k$.

(2) ϕ_k is uniformly distributed from $-\pi$ to π.

Under these assumptions, and additionally letting N tend to infinity, it is seen that r and i are jointly Gaussian random variables. Goodman [1] has derived the statistics of the electric field amplitude and intensity. Letting $\langle \cdot \rangle$ represent an ensemble average (i.e. the average over many independent diffusers) we find the covariance matrix is determined to be

$$M = \begin{bmatrix} \langle rr \rangle & \langle ri \rangle \\ \langle ir \rangle & \langle ii \rangle \end{bmatrix} \tag{3}$$

$$= \begin{bmatrix} \sigma^2 & 0 \\ 0 & \sigma^2 \end{bmatrix}$$

and thus

$$p(r,i) = \frac{1}{2\pi\sigma^2} \exp\{-\frac{r^2+i^2}{2\sigma^2}\} \ . \tag{4}$$

Note that σ^2 can be written as $R_{rr}(\Delta z=0, \Delta y=0)$ where R_{fg} denotes the correlation of f with g. The transformation

$$\begin{aligned} r &= \sqrt{I}\cos(\omega t + \phi) \\ i &= \sqrt{I}\sin(\omega t + \phi) \end{aligned} \tag{5}$$

is used to find

$$p(I) = \frac{1}{2\sigma^2} e^{-\frac{I}{2\sigma^2}} \ . \tag{6}$$

Probability Density Function of Slopes in One Dimension

Higher-order statistics involve the real and imaginary parts of the electric field at more than one point. Our problem concerning the slopes of the real and imaginary parts of the electric field can be treated in the manner of second-order statistics because of the linearity of the derivative process. Initially, the discussion will be restricted to variation in the x-direction only; later, variation in the y-direction will be included as well.

Consider $r(x_1,y,z,t)$, $i(x_1,y,z,t)$, $r(x_2,y,z,t)$, and $i(x_2,y,z,t)$. The central limit theorem tells us they are jointly Gaussian random variables [7]. It is also true that $r(x,y,z,t)$, $\frac{\partial}{\partial x} r(x,y,z,t)$, $i(x,y,z,t)$, and $\frac{\partial}{\partial x} i(x,y,z,t)$ are jointly Gaussian [8, p.475]. As a shorthand notation, $\frac{\partial}{\partial x} f(x,y,z,t)$ will be written as $f_x(x,y,z,t)$. The general form of the distribution density function is [8, p. 255]

$$p(r,i,r_x,i_x) = \frac{1}{4\pi^2\sqrt{\det M}} \exp\{-\frac{1}{2}[u]M^{-1}[u]^T\} \tag{7}$$

where

$$[u] = [\, r \quad i \quad r_x \quad i_x \,] \tag{8}$$

and

$$M = \begin{bmatrix} <rr> & <ri> & <rr_x> & <ri_x> \\ <ir> & <ii> & <ir_x> & <ii_x> \\ <r_xr> & <r_xi> & <r_xr_x> & <r_xi_x> \\ <i_xr> & <i_xi> & <i_xr_x> & <i_xi_x> \end{bmatrix} . \tag{9}$$

Following Ebeling [3] , we note two relations in order to evaluate elements of M:

(1)

$$\begin{aligned} R_{EE}(\Delta x) &= <A(x_1,y,z)A(x_2,y,z)><e^{i2\theta}>e^{i2\omega t} \\ &= 0 \end{aligned} \tag{10}$$

since $<e^{i2\theta}> = 0$. Note $A(x,y,z)$ is the complex amplitude of the electric field given in Eq. (1). Therefore, equating real and imaginary parts, we find that

$$\begin{aligned} R_{rr}(\Delta x) &= R_{ii}(\Delta x) \\ R_{ri}(\Delta x) &= -R_{ir}(\Delta x) \ . \end{aligned} \tag{11}$$

(2) From Papoulis [8, p.317] , with $f^{(n)}$ representing $\frac{\partial^n}{\partial x^n} f$, we have

$$R_{f^{(n)}g^{(m)}}(\Delta x) = (-1)^m \frac{\partial^{(n+m)}}{\partial \Delta x^{(n+m)}} R_{fg}(\Delta x) \ . \tag{12}$$

M is symmetric and the upper $2x2$ portion of it is already known, so seven elements remain to be determined. Note that

$$\langle r_s r_s \rangle = -\frac{\partial^2}{\partial \Delta x^2} R_{rr}(\Delta x)\Big|_{\Delta x=0} \equiv b_s \ . \tag{13}$$

Similarly,

$$\langle i_s i_s \rangle = b_s \ . \tag{14}$$

From Eq. (11), it is seen that

$$\langle r_s i_s \rangle = -\frac{\partial^2}{\partial \Delta x^2} R_{ri}(\Delta x)\Big|_{\Delta x=0} = \frac{\partial^2}{\partial \Delta x^2} R_{ir}(\Delta x)\Big|_{\Delta x=0} = -\langle i_s r_s \rangle \tag{15}$$

and thus

$$\langle r_s i_s \rangle = \langle i_s r_s \rangle = 0 \ .$$

Continuing, since

$$\langle ff \rangle' = \langle (ff)' \rangle = 2\langle ff' \rangle$$

we find

$$\begin{aligned} \langle r r_s \rangle &= \frac{1}{2}\frac{\partial}{\partial x}\langle rr \rangle \\ &= \frac{1}{2}\frac{\partial}{\partial x}(\text{constant}) = 0 \ . \end{aligned} \tag{16}$$

By the same reasoning, $\langle i i_s \rangle = 0$ as well. Finally,

$$\langle r i_s \rangle = -\frac{\partial}{\partial \Delta x} R_{ri}(\Delta x)\Big|_{\Delta x=0} \equiv c_s \tag{17}$$

and $\langle r_s i \rangle$ is simply $-\langle r i_s \rangle$. Therefore,

$$M = \begin{bmatrix} \sigma^2 & 0 & 0 & c_s \\ 0 & \sigma^2 & -c_s & 0 \\ 0 & -c_s & b_s & 0 \\ c_s & 0 & 0 & b_s \end{bmatrix} . \tag{18}$$

From this form, the determinant and inverse of M are found to be

$$\det M = (\sigma^2 b_s - c_s^2)^2 \tag{19}$$

and

$$M^{-1} = \frac{1}{D}\begin{bmatrix} b_s & 0 & 0 & -c_s \\ 0 & b_s & c_s & 0 \\ 0 & c_s & \sigma^2 & 0 \\ -c_s & 0 & 0 & \sigma^2 \end{bmatrix} \tag{20}$$

where

$$D = \sqrt{\det M} = \sigma^2 b_s - c_s^2 \ . \tag{21}$$

Performing the matrix-vector multiplications of Eq. (7), we get

$$p(r,i,r_s,i_s) = \frac{1}{4\pi^2 D}\exp\{-\frac{1}{2D}[b_s(r^2+i^2) + \sigma^2(r_s^2+i_s^2) + 2c_s(ir_s - ri_s)]\} \tag{22}$$

The transformation of variables to intensity I and phase ϕ is

$$\begin{aligned} r &= \sqrt{I}\cos(\omega t+\phi) \\ i &= \sqrt{I}\sin(\omega t+\phi) \\ r_s &= \frac{I_s}{2\sqrt{I}}\cos(\omega t+\phi) - \sqrt{I}\,\phi_s\sin(\omega t+\phi) \\ i_s &= \frac{I_s}{2\sqrt{I}}\sin(\omega t+\phi) + \sqrt{I}\,\phi_s\cos(\omega t+\phi) \\ \|J\| &= \frac{1}{4} \end{aligned} \tag{23}$$

with a resulting probability density function

$$p(I,\phi,I_s,\phi_s) = \frac{1}{16\pi^2 D}\exp\{-\frac{1}{2D}[b_s I + \sigma^2(\frac{I_s^2}{4I} + I\phi_s^2) - 2c_s I\phi_s]\} \ . \tag{24}$$

Since the probability density function of ϕ_s is our goal, it is necessary to integrate over I, ϕ and I_s. This is a straightforward process and results in

$$p(\phi_s) = \frac{1}{2\sigma}\,\frac{(\sigma^2 b_s - c_s^2)}{(\sigma^2\phi_s^2 - 2c_s\phi_s + b_s)^{3/2}} \ . \tag{25}$$

where, to repeat,

$$\begin{aligned} \sigma^2 &= R_{rr}(\Delta z=0) \\ b_s &= -\frac{\partial^2}{\partial\Delta z^2}R_{rr}(\Delta z)\Big|_{\Delta z=0} \end{aligned} \tag{26}$$

$$c_x = -\frac{\partial}{\partial \Delta x} R_{ri}(\Delta x) \Big|_{\Delta x = 0} .$$

This expression can be compared with the distribution obtained in the analogous problem concerning the instantaneous frequency of narrowband Gaussian noise. Blachman's formula [6, p.61] is

$$p(\phi_x) = \frac{2\pi^2\rho^2}{(\phi_x^2 + 4\pi^2\rho^2)^{3/2}} \tag{27}$$

where ρ^2 is the spectral width and is defined as

$$\rho^2 = \frac{1}{4\pi^2} \frac{\langle r_x r_x \rangle}{\sigma^2} . \tag{28}$$

Therefore, the relationship to our notation is

$$b_x = 4\pi\rho^2\sigma^2 \tag{29}$$

In addition, in Blachman's formulation of the problem, $c_x = 0$ because he takes as his reference frequency the centroid of the noise spectrum. Hence, it is seen that the two formulas are equivalent.

Probability Density Function of Slopes in Two Dimensions

Our ultimate goal is to solve the two-dimensional problem, finding an expression for $p(\phi_x, \phi_y)$. This will give us the statistical distribution of geometrical ray directions since, if α and β are the direction cosines with respect to the x- and y-axes, then

$$\phi_x = \frac{2\pi}{\lambda}\alpha \tag{30}$$
$$\phi_y = \frac{2\pi}{\lambda}\beta$$

Extrapolating from the previous section, the desired density function is seen to be obtainable from $p(r, i, r_x, i_x, r_y, i_y)$. By earlier reasoning, these six random variables are jointly Gaussian. Hence, the general form of the distribution is

$$p(r, i, r_x, i_x, r_y, i_y) = \frac{1}{8\pi^3\sqrt{\det M}} \exp\{-\frac{1}{2}[u]M^{-1}[u]^T\} \tag{31}$$

Here,

$$[u] = [\, r \quad i \quad r_x \quad i_x \quad r_y \quad i_y \,] \tag{32}$$

and

$$M = \begin{bmatrix} \langle rr \rangle & \langle ri \rangle & \langle rr_x \rangle & \langle ri_x \rangle & \langle rr_y \rangle & \langle ri_y \rangle \\ \langle ir \rangle & \langle ii \rangle & \langle ir_x \rangle & \langle ii_x \rangle & \langle ir_y \rangle & \langle ii_y \rangle \\ \langle r_x r \rangle & \langle r_x i \rangle & \langle r_x r_x \rangle & \langle r_x i_x \rangle & \langle r_x r_y \rangle & \langle r_x i_y \rangle \\ \langle i_x r \rangle & \langle i_x i \rangle & \langle i_x r_x \rangle & \langle i_x i_x \rangle & \langle i_x r_y \rangle & \langle i_x i_y \rangle \\ \langle r_y r \rangle & \langle r_y i \rangle & \langle r_y r_x \rangle & \langle r_y i_x \rangle & \langle r_y r_y \rangle & \langle r_y i_y \rangle \\ \langle i_y r \rangle & \langle i_y i \rangle & \langle i_y r_x \rangle & \langle i_y i_x \rangle & \langle i_y r_y \rangle & \langle i_y i_y \rangle \end{bmatrix} \tag{33}$$

Because of symmetry, twenty-one elements must be found, of which ten have already been determined. The remainder of the elements are discussed in Appendix A. The resulting covariance matrix has the form

$$M = \begin{bmatrix} \sigma^2 & 0 & 0 & c_x & 0 & c_y \\ 0 & \sigma^2 & -c_x & 0 & -c_y & 0 \\ 0 & -c_x & b_x & 0 & d & 0 \\ c_x & 0 & 0 & b_x & 0 & d \\ 0 & -c_y & d & 0 & b_y & 0 \\ c_y & 0 & 0 & d & 0 & b_y \end{bmatrix} \tag{34}$$

where

$$d \equiv \langle r_x r_y \rangle = -\frac{\partial}{\partial \Delta x} \frac{\partial}{\partial \Delta y} R_{rr}(\Delta x, \Delta y) \Big|_{\substack{\Delta x = 0 \\ \Delta y = 0}} . \tag{35}$$

The inverse of M is

$$M^{-1} = \frac{1}{D}\begin{bmatrix} b_s b_y - d^2 & 0 & 0 & c_y d - b_y c_s & 0 & c_s d - b_s c_y \\ 0 & b_s b_y - d^2 & -(c_y d - b_y c_s) & 0 & -(c_s d - b_s c_y) & 0 \\ 0 & -(c_y d - b_y c_s) & \sigma^2 b_y - c_y^2 & 0 & c_s c_y - \sigma^2 d & 0 \\ c_y d - b_y c_s & 0 & 0 & \sigma^2 b_y - c_y^2 & 0 & c_s c_y - \sigma^2 d \\ 0 & -(c_s d - b_s c_y) & c_s c_y - \sigma^2 d & 0 & \sigma^2 b_s - c_s^2 & 0 \\ c_s d - b_s c_y & 0 & 0 & c_s c_y - \sigma^2 d & 0 & \sigma^2 b_s - c_s^2 \end{bmatrix} \tag{36}$$

where

$$D = \sqrt{\det M} = \sigma^2 b_s b_y - \sigma^2 d^2 - b_s c_y^2 - b_y c_s^2 + 2 c_s c_y d \quad . \tag{37}$$

Substituting into Eq. (31), we obtain

$$p(r, i, r_s, i_s, r_y, i_y) = \frac{1}{8\pi^2 D} \exp\{-\frac{1}{2D}[(b_s b_y - d^2)(r^2 + i^2) + (\sigma^2 b_y - c_y^2)(r_s^2 + i_s^2) + \tag{38}$$
$$(\sigma^2 b_s - c_s^2)(r_y^2 + i_y^2) + 2(c_y d - b_y c_s)(r i_s - i r_s) + 2(c_s d - b_s c_y)(r i_y - i r_y) + 2(c_s c_y - \sigma^2 d)(r_s r_y + i_s i_y)]\}$$

Again, a transformation is needed to get the distribution of I, ϕ, I_s, ϕ_s, I_y, and ϕ_y . The relations are :

$$\begin{aligned} r &= \sqrt{I}\cos(\omega t + \phi) \\ i &= \sqrt{I}\sin(\omega t + \phi) \\ r_s &= \frac{I_s}{2\sqrt{I}}\cos(\omega t + \phi) - \sqrt{I}\,\phi_s \sin(\omega t + \phi) \\ i_s &= \frac{I_s}{2\sqrt{I}}\sin(\omega t + \phi) + \sqrt{I}\,\phi_s \cos(\omega t + \phi) \\ r_y &= \frac{I_y}{2\sqrt{I}}\cos(\omega t + \phi) - \sqrt{I}\,\phi_y \sin(\omega t + \phi) \\ i_y &= \frac{I_y}{2\sqrt{I}}\sin(\omega t + \phi) + \sqrt{I}\,\phi_s \cos(\omega t + \phi) \quad . \end{aligned} \tag{39}$$

The following transformation expressions result :

$$r^2 + i^2 = I$$
$$r_s^2 + i_s^2 = \frac{I_s^2}{4I} + I\phi_s^2$$
$$r_y^2 + i_y^2 = \frac{I_y^2}{4I} + I\phi_y^2$$

$$
\begin{aligned}
r i_x - i r_x &= I\phi_x \\
r i_y - i r_y &= I\phi_y \\
r_x r_y + i_x i_y &= \frac{I_x I_y}{4I} + I\phi_x\phi_y \\
\|J\| &= \frac{1}{8}
\end{aligned}
\tag{40}
$$

The probability density function hence becomes

$$
p(I,\phi,I_x,\phi_x,I_y,\phi_y) = \frac{1}{64\pi^3 D}\exp\{-\frac{1}{2D}[(b_x b_y - d^2)I + (\sigma^2 b_y - c_y^2)(\frac{I_x^2}{4I} + I\phi_x^2) + \tag{41}
$$

$$
\sigma^2 b_x - c_x^2(\frac{I_y^2}{4I} + I\phi_y^2) + 2(c_y d - b_y c_x)I\phi_x + 2(c_x d - b_x c_y)I\phi_y + 2(c_x c_y - \sigma^2 d)(\frac{I_x I_y}{4I} + I\phi_x\phi_y)]\}
$$

Integration over I, ϕ, I_x and I_y is performed in Appendix B. The resulting joint probability density function of the x-derivative of the phase and the y-derivative of the phase is

$$
\begin{aligned}
p(\phi_x,\phi_y) = \frac{D^{3/2}}{\pi\sigma}[&(b_x b_y - d^2) + (\sigma^2 b_y - c_y^2)\phi_x^2 + (\sigma^2 b_x - c_x^2)\phi_y^2 \\
&+ 2(c_y d - b_y c_x)\phi_x + 2(c_x d - b_x c_y)\phi_y + 2(c_x c_y - \sigma^2 d)\phi_x\phi_y]^{-2} \ .
\end{aligned}
\tag{42}
$$

Examples

It is instructive to calculate $p(\phi_x,\phi_y)$ for some basic intensity distributions at the scattering plane. The parameters of the distribution in Eq. (42) depend on spatial correlation functions. It is possible to rewrite them all as depending on the autocorrelation function of the complex amplitude $R_{AA^*}(\Delta x,\Delta y)$. This can be seen by first noting that

$$
R_{EE^*}(\Delta x,\Delta y) = R_{AA^*}(\Delta x,\Delta y) \tag{43}
$$

By expanding E in terms of its real and imaginary parts, the following relations result :

$$
\begin{aligned}
R_{rr}(\Delta x,\Delta y) &= \frac{1}{2}\mathrm{Re}\, R_{AA^*}(\Delta x,\Delta y) \\
R_{ri}(\Delta x,\Delta y) &= -\frac{1}{2}\mathrm{Im}\, R_{AA^*}(\Delta x,\Delta y) \ .
\end{aligned}
\tag{44}
$$

Hence,

$$
\begin{aligned}
\sigma^2 &= \frac{1}{2}\mathrm{Re}R_{AA^*}(\Delta x{=}0,\Delta y{=}0) \\
b_x &= -\frac{1}{2}\mathrm{Re}\left[\frac{\partial^2}{\partial\Delta x^2}R_{AA^*}(\Delta x,\Delta y)\Big|_{\substack{\Delta x=0\\ \Delta y=0}}\right]
\end{aligned}
$$

$$
\begin{aligned}
c_x &= \frac{1}{2}\mathrm{Im}\left[\frac{\partial}{\partial \Delta x} R_{AA^*}(\Delta x,\Delta y)\Big|_{\substack{\Delta x=0\\ \Delta y=0}}\right] \\
b_y &= -\frac{1}{2}\mathrm{Re}\left[\frac{\partial^2}{\partial \Delta y^2} R_{AA^*}(\Delta x,\Delta y)\Big|_{\substack{\Delta x=0\\ \Delta y=0}}\right] \\
c_y &= \frac{1}{2}\mathrm{Im}\left[\frac{\partial}{\partial \Delta y} R_{AA^*}(\Delta x,\Delta y)\Big|_{\substack{\Delta x=0\\ \Delta y=0}}\right] \\
d &= -\frac{1}{2}\mathrm{Re}\left[\frac{\partial^2}{\partial \Delta x \partial \Delta y} R_{AA^*}(\Delta x,\Delta y)\Big|_{\substack{\Delta x=0\\ \Delta y=0}}\right] .
\end{aligned} \tag{45}
$$

The last relation needed to calculate $p(\phi_x,\phi_y)$ is provided by the Van Cittert-Zernike theorem [9],

$$
R_{AA^*}(\Delta x,\Delta y) = \frac{1}{\lambda^2 z^2} FT_2\{I(u,v)\}_{\frac{\Delta x}{\lambda z},\frac{\Delta y}{\lambda z}} \tag{46}
$$

where FT_2 denotes 2-D Fourier transformation, $I(u,v)$ is the illumination intensity distribution at the scattering plane, and z is the distance between the scattering plane and the observation plane. Combining the results of equations (45) and (46), we find

$$
\begin{aligned}
\sigma^2 &= \frac{1}{2\lambda^2 z^2}\int_0^\infty\int I(u,v)\,du\,dv \\
b_x &= \frac{2\pi^2}{\lambda^4 z^4}\int_0^\infty\int u^2 I(u,v)\,du\,dv \\
c_x &= \frac{\pi}{\lambda^2 z^3}\int_0^\infty\int u I(u,v)\,du\,dv \\
b_y &= \frac{2\pi^2}{\lambda^4 z^4}\int_0^\infty\int v^2 I(u,v)\,du\,dv \\
c_y &= \frac{\pi}{\lambda^2 z^3}\int_0^\infty\int v I(u,v)\,du\,dv \\
d &= \frac{2\pi^2}{\lambda^4 z^4}\int_0^\infty\int uv I(u,v)\,du\,dv \quad .
\end{aligned} \tag{47}
$$

As a first example, consider a rectangular spot of dimension LxW . The intensity distribution is written as

$$
I(u,v) = a\ \mathrm{rect}\left(\frac{u}{L}\right)\mathrm{rect}\left(\frac{v}{W}\right) \tag{48}
$$

where a is a constant and rect (f) is defined to be

$$\text{rect}(f) = \begin{cases} 1 & \text{for } |f| < \frac{1}{2} \\ 0 & \text{for } |f| \geq \frac{1}{2} \end{cases} . \tag{49}$$

Taking the Fourier transform, we obtain

$$R_{AA^*}(\Delta x, \Delta y) = a \frac{LW}{\lambda^2 z^2} \text{sinc}\left(\frac{L}{\lambda z}\Delta x\right) \text{sinc}\left(\frac{W}{\lambda z}\Delta y\right) \tag{50}$$

where

$$\text{sinc}(f) = \frac{\sin(\pi f)}{\pi f}$$

It is convenient to define a "speckle width", in each direction, as the distance in which the correlation function falls to zero. Let

$$\begin{aligned} \delta x &= \text{speckle width in x-direction} = \frac{\lambda z}{L} \\ \delta y &= \text{speckle width in y-direction} = \frac{\lambda z}{W} . \end{aligned} \tag{51}$$

Then

$$R_{AA^*}(\Delta x, \Delta y) = \frac{a}{(\delta x)(\delta y)} \text{sinc}\left(\frac{\Delta x}{\delta x}\right) \text{sinc}\left(\frac{\Delta y}{\delta y}\right) . \tag{52}$$

The parameters needed for Eq. (42) are determined from this equation to be

$$\begin{aligned} \sigma^2 &= \frac{a}{2(\delta x)(\delta y)} \\ b_x &= \frac{a\pi^2}{6(\delta x)^2(\delta y)} \\ c_x &= 0 \\ b_y &= \frac{a\pi^2}{6(\delta x)(\delta y)^2} \\ c_y &= 0 \\ d &= 0 . \end{aligned} \tag{53}$$

Hence,

$$p(\phi_x, \phi_y) = \frac{\pi}{3(\delta x)^3(\delta y)^3} \left[\frac{\phi_x^2}{(\delta y)^2} + \frac{\phi_y^2}{(\delta x)^2} + \frac{\pi^2}{3(\delta x)^2(\delta y)^2}\right]^2 . \tag{54}$$

If $L = W$ (and therefore $\delta x = \delta y$),

$$p(\phi_x,\phi_y) = \frac{\pi}{3(\delta x)^2}\left[\phi_x^2 + \phi_y^2 + \frac{\pi^2}{3(\delta x)^2}\right]^{-2} . \tag{55}$$

A graph of this function is shown in Fig. 1. for the following parameters:

$$\begin{aligned} \lambda &= .5 \cdot 10^{-6}\ \text{m} \\ z &= 1\ \text{m} \\ L &= 1\ \text{mm} \\ \delta x &= .0005\ \text{m} \end{aligned} \tag{56}$$

Both ϕ_x and ϕ_y range from -10,000 to 10,000 radians per meter with the (0,0) point at the center of the graph.

As a second example, a symmetric Gaussian scattering spot is considered. The intensity distribution,

$$I(u,v) = a\, e^{-\frac{u^2+v^2}{L^2/4}} , \tag{57}$$

is defined so that $L/2$ is the $1/e$ point in each direction. The autocorrelation function is

$$R_{AA}(\Delta x,\Delta y) = a\pi \frac{L^2}{4\lambda^2 z^2} \exp\left\{-\pi^2(\Delta x^2+\Delta y^2)\frac{L^2}{4\lambda^2 z^2}\right\} . \tag{58}$$

Let the definition of speckle width in this case be the $1/e$ point. Thus

$$\delta x = \delta y = \frac{2\lambda z}{L\pi}$$

and the nonzero parameters of $p(\phi_x,\phi_y)$ are found to be

$$\begin{aligned} \sigma^2 &= \frac{a}{2\pi(\delta x)^2} \\ b_x &= \frac{a}{\pi(\delta x)^4} = b_y . \end{aligned} \tag{59}$$

The resulting distribution density is

$$p(\phi_x,\phi_y) = \frac{2}{\pi(\delta x)^2}\left[\phi_x^2 + \phi_y^2 + \frac{2}{(\delta x)^2}\right]^{-2} . \tag{60}$$

Conclusion

The joint probability density function of the x- and y- components of the phase in a monochromatic, fully developed speckle pattern has been found. Equivalently, the statistical distribution of ray directions in such a speckle pattern have been derived. The results show that the statistics in question depend on only the two first and three second spatial moments of the illumination distribution of the scattering object but not on other details of that distribution. This problem is the two-dimensional analog of the problem of finding the statistics of the instantaneous frequency of narrowband Gaussian random noise. The results should prove useful in studies of the average diffraction efficiency of thick holograms of diffuse objects and may be of interest in adaptive optics.

Acknowledgments

The authors gratefully acknowledge support from AFOSR and an IBM predoctoral fellowship.

Appendix A

The 6x6 covariance matrix M (Eq. (33) in the main text) has, on account of symmetry, twenty-one distinct elements which must be found. Ten of these were discussed in the text. Furthermore, seven more have exact analogies to cases previously studied. Thus :

$$\langle r_y r_y \rangle = -\frac{\partial^2}{\partial \Delta y^2} R_{rr}(\Delta y)\Big|_{\Delta y=0} \equiv b_y \tag{61}$$

and $\langle i_y i_y \rangle = b_y$ as well;

$$\langle r_y i_y \rangle = 0 \tag{62}$$

$$\langle r r_y \rangle = \langle i i_y \rangle = 0 \tag{63}$$

$$\langle r i_y \rangle = -\frac{\partial}{\partial \Delta y} R_{ri}(\Delta y)\Big|_{\Delta y=0} \equiv c_y \tag{64}$$

and $\langle r_y i \rangle = -\langle r i_y \rangle$.

To study the remaining four covariances, it is necessary to find a relation similar to Eq. (12), but where the partial derivatives of the two functions to be cross-correlated are with respect to two different variables.

Following the reasoning of Papoulis [8, p.316], we can evaluate

$$R_{f_x g_y}(x_1,x_2,y_1,y_2) = E\{f_x(x_1,y_1)g_y(x_2,y_2)\} \tag{65}$$

in two separate steps. First, we observe that

$$E\left\{f(x_1,y_1)\left[\frac{g(x_2,y_2+\epsilon)-g(x_2,y_2)}{\epsilon}\right]\right\} = \frac{R_{fg}(x_1,x_2,y_1,y_2+\epsilon)-R_{fg}(x_1,x_2,y_1,y_2)}{\epsilon} \tag{66}$$

Taking the limit of both sides as $\epsilon \to 0$, we get

$$R_{fg_y}(x_1,x_2,y_1,y_2) = \frac{\partial}{\partial y_2} R_{fg}(x_1,x_2,y_1,y_2) \tag{67}$$

Second,

$$E\left\{\left[\frac{f(x_1+\epsilon,y_1)-f(x_1,y_1)}{\epsilon}\right] g_y(x_2,y_2)\right\} = \frac{R_{fg_y}(x_1+\epsilon,x_2,y_1,y_2)-R_{fg_y}(x_1,x_2,y_1,y_2)}{\epsilon} \tag{68}$$

Again taking the limit as $\epsilon \to 0$, we find

$$\begin{aligned} R_{f_x g_y}(x_1,x_2,y_1,y_2) &= \frac{\partial}{\partial x_1} R_{fg_y}(x_1,x_2,y_1,y_2) \\ &= \frac{\partial}{\partial x_1}\frac{\partial}{\partial y_2} R_{fg}(x_1,x_2,y_1,y_2) \end{aligned} \tag{69}$$

If the processes are jointly spatially stationary, then

$$R_{f_x g_y}(\Delta x,\Delta y) = -\frac{\partial}{\partial \Delta x}\frac{\partial}{\partial \Delta y} R_{fg}(\Delta x,\Delta y) \tag{70}$$

where

$$\begin{aligned} \Delta x &= x_1 - x_2 \\ \Delta y &= y_1 - y_2 \end{aligned} \tag{71}$$

Returning to the remaining covariance terms, we have

$$\langle r_x i_y \rangle = -\frac{\partial}{\partial \Delta x}\frac{\partial}{\partial \Delta y} R_{ri}(\Delta x,\Delta y) = \frac{\partial}{\partial \Delta x}\frac{\partial}{\partial \Delta y} R_{ir}(\Delta x,\Delta y) = -\langle i_y r_x \rangle \tag{72}$$

and so

$$<r_s i_y> = <i_y r_s> \equiv 0 \ . \tag{73}$$

Lastly,

$$<r_s r_y> = -\frac{\partial}{\partial \Delta x}\frac{\partial}{\partial \Delta y} R_{rr}(\Delta x, \Delta y)\Big|_{\substack{\Delta x=0 \\ \Delta y=0}} = d \tag{74}$$

and $<i_x i_y> = <r_x r_y>$. The resulting covariance matrix is given in Eq. (34) of the main text.

Appendix B

The probability density function obtained when the transformation to six variables related to intensity and phase is completed is, as given in Eq. (41) of the main text,

$$p(I,\phi,I_x,\phi_x,I_y,\phi_y) = \frac{1}{64\pi^3 D}\exp\{-\frac{1}{2D}[(b_x b_y - d^2)I + (\sigma^2 b_y - c_y^2)(\frac{I_x^2}{4I} + I\phi_x^2) +$$

$$\sigma^2 b_x - c_x^2(\frac{I_y^2}{4I} + I\phi_y^2) + 2(c_y d - b_y c_x)I\phi_x + 2(c_x d - b_x c_y)I\phi_y + 2(c_x c_y - \sigma^2 d)(\frac{I_x I_y}{4I} + I\phi_x\phi_y)]\} \ .$$

Integration over ϕ yields a factor of 2π . The integration over I_x is of the form

$$\int_{-\infty}^{\infty} e^{-(ax^2+bx)}dx = \sqrt{\frac{\pi}{a}}e^{\frac{b^2}{4a}}$$

where

$$a = \frac{\sigma^2 b_y - c_y^2}{8ID} \qquad b = \frac{(c_x c_y - \sigma^2 d)I_y}{4ID} \ . \tag{75}$$

The form of the integration over I_y is then simply

$$\int_{-\infty}^{\infty} e^{-ax^2}dx = \sqrt{\frac{\pi}{a}} \quad \text{with} \quad a = \frac{1}{2D}\left[\frac{\sigma^2 b_x - c_x^2}{4I} - \frac{(c_x c_y - \sigma^2 d)^2}{4I(\sigma^2 b_y - c_y^2)}\right] \ . \tag{76}$$

It is useful to note that

$$(\sigma^2 b_x - c_x^2)(\sigma^2 b_y - c_y^2) - (c_x c_y - \sigma^2 d)^2 = \sigma^2 D \tag{77}$$

so a can be rewritten as

$$a = \frac{\sigma^2}{8I(\sigma^2 b_y - c_y^2)} \ . \tag{78}$$

These integrations leave

$$p(I,\phi_x,\phi_y) = \frac{I}{4\pi\sigma\sqrt{D}}\exp\{-\frac{I}{2D}[(b_x b_y - d^2) + (\sigma^2 b_y - c_y^2)\phi_x^2 + (\sigma^2 b_x - c_x^2)\phi_y^2 + 2(c_y d - b_y c_x)\phi_x + 2(c_x d - b_x c_y)\phi_y + 2(c_x c_y - \sigma^2 d)\phi_x\phi_y]\} \quad . \tag{79}$$

The last integration takes the form

$$\int_0^\infty I e^{-aI}\,dI = \frac{\Gamma(2)}{a^2} = \frac{1}{a^2} \quad . \tag{80}$$

Finally, the joint probability density function of the x-derivative of the phase and the y-derivative of the phase is

$$p(\phi_x,\phi_y) = \frac{D^{3/2}}{\pi\sigma}[(b_x b_y - d^2) + (\sigma^2 b_y - c_y^2)\phi_x^2 + (\sigma^2 b_x - c_x^2)\phi_y^2 + 2(c_y d - b_y c_x)\phi_x + 2(c_x d - b_x c_y)\phi_y + 2(c_x c_y - \sigma^2 d)\phi_x\phi_y]^{-2} \quad .$$

References

1. Joseph W. Goodman, "Statistical Properties of Laser Speckle Patterns," in *Laser Speckle and Related Phenomena*, ed. J.C. Dainty,Springer-Verlag (1975).
2. J. Christopher Dainty, "The Statistics of Speckle Patterns," pp. 1-46 in *Progress in Optics, Vol. 14*, ed. Emil Wolf,North-Holland Publishing Co., Amsterdam (1977).
3. K.J. Ebeling, "Statistical properties of spatial derivatives of the amplitude and intensity of monochromatic speckle patterns," *Optica Acta* 26(2) p. 1505 (1979).
4. Junji Ohtsubo, "Exact Solution of the Zero Crossing Rate of a Differentiated Speckle Pattern," *Optics Communications* 42(1) p. 13 (1982).
5. M.S. Longuet-Higgins, "The Statistical Analysis of a Random, Moving Surface," *Philosophical Transactions, Series A* 249 p. 321 (1957).
6. Nelson M. Blachman, *Noise and Its Effect on Communication*, McGraw-Hill, Inc., New York (1966).
7. D. Middleton, *An Introduction to Statistical Communication Theory*, McGraw-Hill Book Co., New York (1960).
8. A. Papoulis, *Probability, Random Variables, and Stochastic Processes*, McGraw-Hill, Inc., New York (1965).
9. Max Born and Emil Wolf, *Principles of Optics, 2nd rev. ed.*, Pergamon Press, New York (1964).
10. An alternative way of setting up the problem presented in this paper is to define the axes of the system in terms of the intensity distribution $I(u,v)$. If we choose its centroid as our origin, Eq. (47) tells us that c_x and c_y are zero. In addition, d will be zero if the x and y axes are aligned with the principal axes of the scattering surface, i.e. the directions along the maximum and minimum of the second moment ellipse. The resulting covariance matrix and probability density function are simpler in form. We appreciate the comments of Nelson Blachman on this point.

Figure Captions

Fig. 1 : Joint probability density function of the x- and y- derivatives of the phase for a uniform, square intensity spot in the scattering plane.

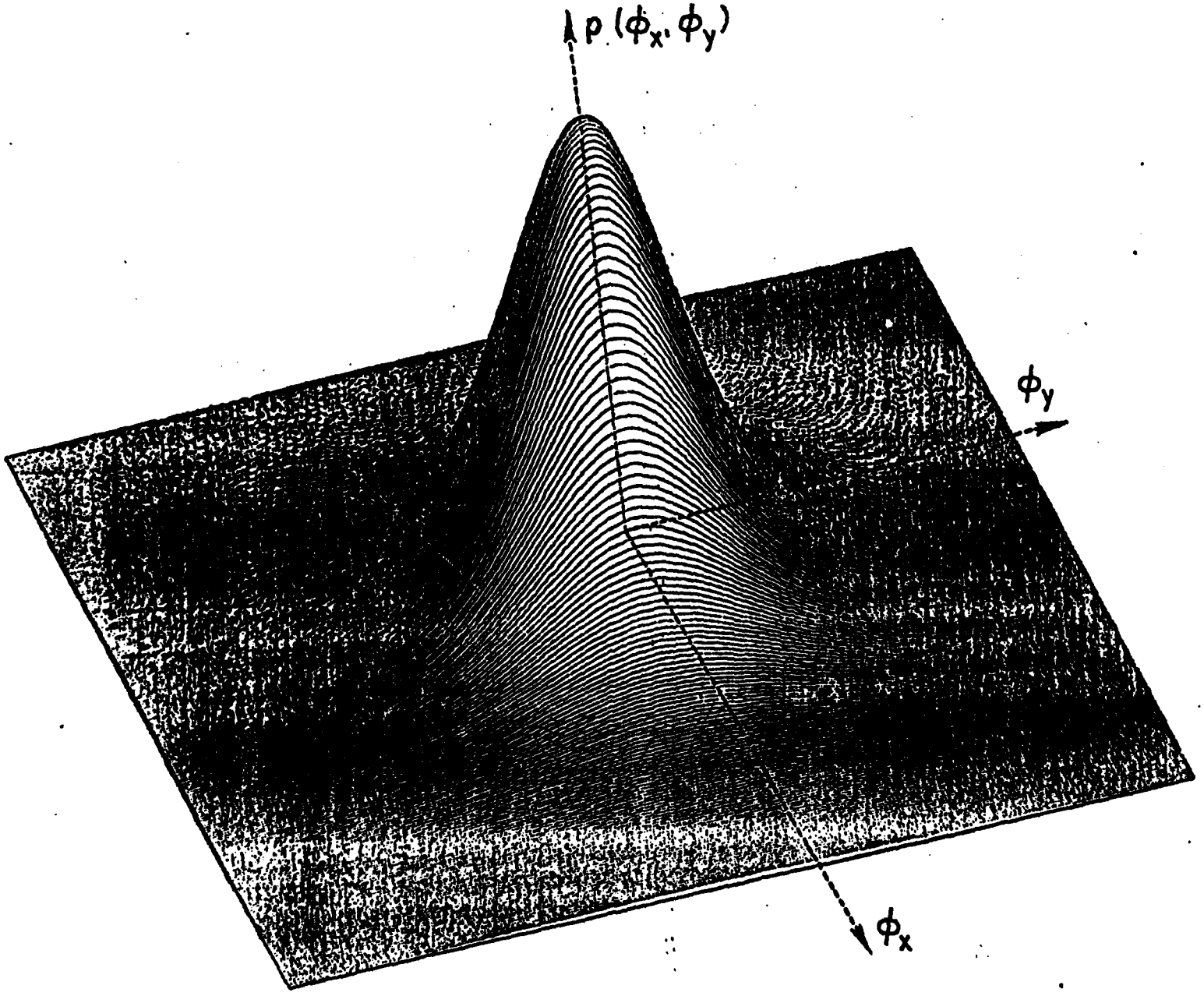
p (φx, φy)
φy
φx

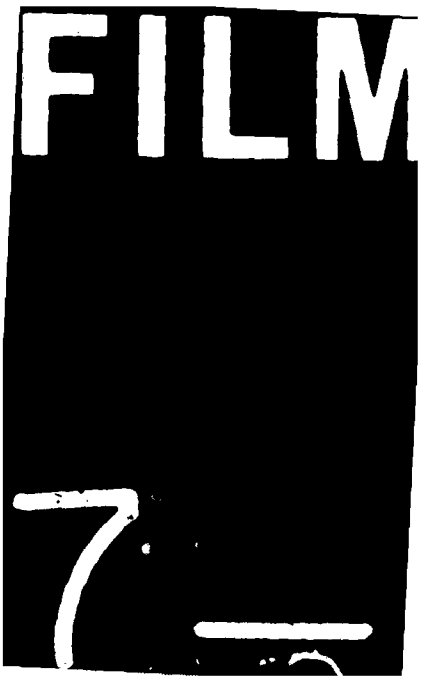
FILM
7